AN ABSTRACT OF THE THESIS OF

Jinwon Kim for the degree of Master of Science

in Atmospheric Sciences presented on May 9, 1986

Title: The Effects of an Isolated Mesoscale Island on a Stably-stratified Airstream

Abstract approved: Redacted for Privacy

James W. Deardorff

The perturbation of a stably-stratified flow by irregular terrain is studied utilizing a seven-layer, hydrostatic, and potential enstrophy and energy conserving primitive equation model. The Island of Oahu, Hawaii, and the surrounding ocean area of 130 km x100km is chosen as the model topography. The domain is covered with a 5km x 5 km mesh of 26 x 20 grid points in the horizontal. A cyclic boundary condition is imposed at the lateral boundaries. In order to give finer resolution to the lower atmosphere, an irregularly spaced sigma-coordinate is used in the vertical. Uniform east-north-easterly large-scale geostrophic winds up to the 400mb level are imposed in order to represent the typical trade-wind condition.

The pressure perturbation related to the mass flux divergence associated with the terrain irregularities, and the land-sea temperature difference associated with the different responses to the insolation during the daytime, are found to play a key role in determining the velocity field in the horizontal as well as in the vertical. Asymmetric surface pressure arises, due to the

topographically induced vertical motion, with high pressure at the windward slope and low pressure at the downwind slope of the island.

Daytime heating of the island induces low pressure on the island surface. This effect is the most significant at the lee side and inland portion of the island where the effect of cold-air advection from the ocean is minimal. At the lee side of the island the negative pressure perturbation induced by the daytime heating favors the establishment of a reverse flow toward the island, but the mountain range at the lee side of the island and prevailing tradewind prevent this low-level inflow from penetrating further inland. At the upwind side of the island, the flow field is mostly determined by topographic slope rather than by the heating of the island surface.

The perturbation to the basic flow decreases rapidly upward. But a vertical cross-section of the horizontal divergence and the vertical velocity fields shows well defined wave motions up to the domain top level. The wave motions also appear downstream and upstream of the island with reduced amplitudes away from the island. These suggest the existence of hydrostatic mountain waves forced by the island contour, as was predicted by previous linear studies. The windward tilt of the wave axis shows upward propagation of wave energy, but the wave momentum flux was negligible.

The Effects of an Isolated Mesoscale Island on a Stably-stratified Airstream

by

Jinwon Kim

A THESIS

submitted to

Oregon State University

in partial fulfillment of

the requirements for the

degree of

Master of Science

Completed May 9, 1986

Commencement June 1987

APPROVED:

Redacted for Privacy

Professor of Atmospheric Sciences in charge of major

Redacted for Privacy

Chairperson of the Department of Atmospheric Sciences

Redacted for Privacy

Dean of Graduate School

Date thesis is presented May 9, 1986

Typed by researcher Jinwon Kim

ACKNOWLEDGEMENTS

I am deeply indebted to Prof. James W. Deardorff for his invaluable guidance and support throughout the course of my study. As my major professor, he was extremely inspiring and helpful to me. I also owe great appreciation to Dr. Young-June Han for his thoughtful comments and helpful discussions on this study. Without their guidance and support, I could never have finished this study.

William McKie provided indispensible assistance on the computing and communication with NASA. I also appreciate the help of Ben Santer for his reading of the manuscript and suggesting improvements in the use of the English language. Thanks to Ms. Monica Rose Cox for typing the final manuscript.

Special thanks to my parents and friends. They eagerly sent help when I needed it. Their encouragement and care was a great mental support for me. I also say thanks to my teachers. They taught and showed me how to think about the problems which we encounter in our environment.

This study was supported by NASA contract #NAG 5-51.

TABLE OF CONTENTS

LIST OF FIGURES

THE EFFECTS OF AN ISOLATED MESOSCALE ISLAND ON A STABLY-STRATIFIED AIRSTREAM

INTRODUCTION

The effects of uneven terrain and land-sea temperature contrast are important in determining the disturbances to the airstream in the vicinity of an island. The importance of the topographic slopes is that the atmosphere is quite sensitive to vertical motions. When the flow over topographic slopes is displaced vertically in the presence of stable stratification, buoyancy forces will try to bring the vertically displaced air parcels to their equilibrium levels even if such restoration requires strong disturbances of the basic flow.

Problems of this kind have been under intense study for two-dimensional topography, but only a few studies have considered three-dimensional topography. The most significant difference between two- and three-dimensional cases is that lateral dispersion of the incoming flow around the topography is possible for three-dimensional topographic barrier. Wurtele (1957) and Smith (1980) have shown that unlike the two-dimensional case, the nodal lines of the resulting disturbances are hypobolas in horizontal planes, as often observed downstream of isolated mountain profiles. But it has been also shown by Wurtele (1957) that the disturbances generated by a three-dimensional topographic barrier are quite similar to those by a two-dimensional one in a

vertical plane which is parallel to the direction of the mean flow.

For a topography whose length scale is less than 50 km with a mean-flow speed of 10 m/sec, transient effects of the earth's rotation are negligible. Hence the resulting disturbances near the topographic barrier do not have sufficient time for geostrophic adjustment. In such a flow, the amount of vertical displacement of air parcels is controlled by the Froude number, $Fr=U/Nh$ (Smith, 1980; Pierrehumbert and Wyman, 1985). For $Fr>>1$, i.e., strong wind and weak stratification, vertical displacement of streamlines is possible and an asymmetric surface pressure arises with high pressure at the upslopes and low pressure at the downslopes. The high pressure at the upslope causes the incoming flow to diverge laterally, and the low pressure at the lee slope induces convergence. This asymmetric surface pressure results in mountain drag and is associated with generation of vertically propagating waves (Eliassen and Palm, 1961; Smith, 1980). For $Fr<<1$, weak wind and strong stratification, vertical displacement of fluid parcels is strongly prohibited by buoyancy force and the flow becomes essentially two-dimensional. For this limit, Drazin (1961) has shown that for a hemispheric obstacle the primary velocity is horizontal, but the secondary velocity has a vertical as well as a horizontal component. He has also shown that the vertical displacement of streamlines and the horizontal pressure

perturbation are fore-aft symmetric with maximum values at the upwind and downwind slopes and minimum values at the left- and right-hand sides of the obstacle with respect to the incoming flow. There is, consequently, no mountain drag or mountain waves.

Once wave energy is generated, it propagates upward or it is trapped in the lower atmosphere. The vertical propagation of wave energy depends on the vertical distributions of the static stability and mean wind speed of the overlying atmosphere through the Scorer number ℓ, where $\ell^2 = N^2/U^2 - U_{zz}/U$. Wurtele (1957) has shown that for $k^2 < \ell^2$, where k is the horizontal wave number in the direction of the mean flow, the resulting waves are of internal type and can propagate upward. Klemp and Lilly (1975) have shown that for decreasing ℓ^2 with height, reflection of wave energy at the higher levels is possible and can cause strong low-level disturbances such as gusty winds often observed at the downslopes of the major mountain ranges. They also have shown that the maximum intensity of the low-level disturbances takes place when the phase shift across the troposphere is close to one-half wavelength.

With intense daytime solar heating, the sea-surface temperature changes quite less than the ground-surface temperature. Sensible heat flux from the underlying ground surface causes an increase of overlying mixed-layer temperature. For a thermal forcing confined to the ground surface and whose

time scale is less than a day, the effect of the heating is mostly confined to the lower atmosphere. For this case, the effect of the land-sea temperature contrast results in the formation of a surface-pressure difference between the land and ocean surfaces, with low pressure at the land surface and high pressure at the ocean surface. A sea-breeze circulation is a quite well known response of the lower atmosphere to the land-sea temperature contrast and associated surface-pressure perturbations. This sea-breeze circulation brings cool air from the ocean surface toward the land and hence acts to reduce the existing low-level temperature contrast between the land and sea surfaces.

In the presence of mean flow which is quite steady in direction and magnitude, the mixed-layer temperature distribution over the island along the mean flow direction has an asymmetric structure, with high temperature at the lee side and low temperature at the windward side. This is so because the cool air from the ocean surface is gradually heated while flowing over the heated surface. Hence the effects of the cold-air advection by the mean flow is less at the lee side than at the windward side. By the effects of this differential temperature advection by the mean flow, the low pressure at the lee side is further intensified while the high pressure at the windward side is less changed.

The purpose of the present study is to gain a better understanding of the nature of the disturbances generated by a

three-dimensional topographic barrier subject to daytime heating. Realistic orography of the island of Oahu, Hawaii, was utilized as the model orography. Realistic topography generates complicated disturbances in the flow fields and hence makes it difficult to investigate the detailed response of the topographic barrier. But existence of climatological data enables us to compare and evaluate the model results against the observed data, although exact comparison between those two fields is not possible.

In Chapter 2, brief explanations of the features of the present numerical model and the experimental designs for this study will be presented. In Chapter 3, the results of the numerical study will be presented and analyzed. And the discussions and conclusions of this study will be given in Chapter 4.

CHAPTER 2

2-1 Model

Because details of the model have been reported by K.Ueyoshi (1985), only a brief description and recent changes to the model will be presented here. The most important change to the model is the inclusion of horizontal diffusion in calculating the horizontal velocity field and the potential temperature field. Major features of the seven layer model are;

i) the potential-enstrophy conserving finite-difference scheme developed by Suarez and Arakawa (1979)

ii) the adiabatic reference atmosphere proposed by Phillips (1974) to reduce truncation error in the pressure-gradient force term

iii) bulk transfer coefficients based on the formulation of Louis (1979) that requires no special treatment for the free convection regime and also is appropriate for very stable conditions

iv) horizontal eddy diffusion based on the formulation of Smagorinsky (1963), and

v) the energy-balance equation between heat flux at the surface and the net radiation to determine the ground-surface temperature.

I) Basic equations

* Horizontal momentum equations

$$\frac{\partial u}{\partial t} + \dot{\sigma}\frac{\partial u}{\partial \sigma} - q\pi v + \frac{1}{2}\frac{\partial}{\partial x}(u^2+v^2) = -\left(\frac{\partial \phi}{\partial x}\right)_p - f v_g + \frac{g}{\pi}\frac{\partial \tau_x}{\partial \sigma} + \nabla_H \cdot (K_H \nabla_H u) \tag{2.1}$$

$$\frac{\partial v}{\partial t} + \dot{\sigma}\frac{\partial v}{\partial \sigma} + q\pi u + \frac{1}{2}\frac{\partial}{\partial y}(u^2+v^2) = -\left(\frac{\partial \phi}{\partial y}\right)_p + f u_g + \frac{g}{\pi}\frac{\partial \tau_y}{\partial \sigma} + \nabla_H \cdot (K_H \nabla_H v) \tag{2.2}$$

where

$$-\nabla_p = -\nabla_\sigma + \frac{\sigma}{\pi}\nabla\pi\frac{\partial}{\partial \sigma} \tag{2.3}$$

* First law of thermodynamics for a dry atmosphere

$$\frac{\partial}{\partial t}(\pi\theta) + \nabla_\sigma \cdot (\pi\theta\vec{V}) + \frac{\partial}{\partial \sigma}(\pi\theta\dot{\sigma}) = \frac{g}{c_p}\frac{\partial H}{\partial \sigma} + \nabla_H \cdot [K_H \nabla_H (\pi\theta)] \tag{2.4}$$

* Equation of state

$$\alpha = c_p \theta \frac{dP}{dp} \tag{2.5}$$

$$P \equiv \left(\frac{p}{p_{oo}}\right)^\kappa \tag{2.6}$$

* Hydrostatic equation

$$d\phi = -c_p \theta \, dP \tag{2.7}$$

* Continuity equation

$$\frac{\partial \pi}{\partial t} + \nabla_\sigma \cdot (\pi \vec{V}) + \frac{\partial}{\partial \sigma}(\pi\dot{\sigma}) = 0 \tag{2.8}$$

with the boundary conditions

$$\pi\dot{\sigma} = 0 \qquad at \quad \sigma = 0, 1 \tag{2.9}$$

Integrating (2.8) with the boundary conditions (2.9) we have

$$\frac{\partial p_s}{\partial t} = -\nabla_\sigma \cdot \int_0^1 \pi \vec{V} \, d\sigma \tag{2.10}$$

* Energy balance equation

$$\epsilon_g \sigma_{ST} T_s^4 + H_{ST} + L \cdot E - (1-A) S^{\downarrow} - \epsilon_a R_L^{\downarrow} = G \tag{2.11}$$

The symbols used above have the following meaning:

u: grid-volume mean east-west direction velocity component

v: grid-volume mean north-south direction velocity component

$\vec{V}$: grid-volume mean horizontal velocity vector

θ: grid-volume mean potential temperature

C_p: specific heat at constant pressure

α: specific volume

K_H: horizontal eddy diffusivity

ζ_x: east-west direction frictional stress

ζ_y: north-south direction frictional stress

p: pressure

p_T: pressure at the top of the domain

p_s: pressure at the surface topography

q: potential vorticity $\equiv \frac{\zeta + f}{h}$

f: Coriolis parameter

u_g: east-west direction geostrophic wind (large-scale)

v_g: north-south direction geostrophic wind (large-scale)

g: gravity

H: vertical eddy heat flux

H_{ST}: sensible heat flux from the ground surface (positive upward)

ε_g: emissivity of the ground surface

σ_{ST}: Stefan-Boltzman constant

A: albedo of the ground surface

ε_a: absorptivity of the ground surface

$R_L^{\downarrow}$: downward long-wave radiation

T_s: ground-surface temperature

E: evaporation rate (Kg/s)

G: ground heat flux (positive upward)

L: latent heat of evaporation

$S^{\downarrow}$: insolation at the ground surface

ϕ: perturbation geopotential

ζ: grid-volume mean relative vorticity

$\pi = p_s - p_T$

$\sigma = (p - p_T) / \pi$

$\dot{\sigma} = d\sigma/dt$

II) Parameterization of the vertical and horizontal turbulent fluxes.

The vertical turbulent flux in the boundary layer depends strongly on the static stability of the flow inside the boundary layer. The buoyancy force would inhibit or enhance the vertical motion according to stable or unstable stratification. The Monin-Obukhov (1954) similarity hypothesis suggests that the vertical turbulent flux can be related to the mean vertical gradient of flow speed and temperature by a function of the stability parameter in the turbulent surface layer. Following the Monin-Obukhov similarity hypothesis, we can write the relationship between the gradient of the mean velocity and temperature and the frictional velocity and the scaling temperature in general form as follows:

$$\frac{kz}{u_*}\frac{\partial \bar{u}}{\partial z} = \phi_M(\zeta) \qquad (2.12)$$

$$\frac{kz}{u_*}\frac{\partial \bar{\theta}}{\partial z} = \phi_H(\zeta) \qquad (2.13)$$

k: von-Karman constant

ζ: stability parameter

L: Monin-Obukhov length scale

z: height

$\bar{u}, \bar{\theta}$: grid-area mean wind speed and potential temperature

The friction velocity u_* and the scaling temperature θ_* are defined in terms of the mean surface turbulent fluxes of momentum

and sensible heat as follows;

$$u_*^2 = -\overline{u'w'} \tag{2.14}$$

$$u_*\theta_* = -\overline{w'\theta'} \tag{2.15}$$

where the primed variables denote the deviation of velocity and temperature from the time averaged values and ($\bar{}$) denotes a grid-area average. To relate the mean vertical turbulent fluxes $\frac{\tau}{\rho}$, $\frac{H}{\rho C_p}$ across the surface layer to the mean variables, the bulk aerodynamic formulation (Deardorff, 1968) was used.

$$\frac{\tau}{\rho} \equiv \overline{u'w'}_s = -C_D u^2(z) \tag{2.16}$$

$$\frac{H}{\rho C_p} \equiv \overline{\theta'w'}_s = -C_H u(z)\left[\theta(z) - \theta_s\right] \tag{2.17}$$

where C_D and C_H are bulk transfer coefficients for momentum and sensible heat, and z is height of the measurement, respectively. In the model calculation, z has been taken to be the height at the middle of the lowest layer, and C_D and C_H are determined accordingly. Combining Eqns. (2.14) with (2.16), and (2.15) with (2.17) we have;

$$C_D = \frac{u_*^2}{u^2(z)} \tag{2.18}$$

$$C_H = \frac{u_*\theta_*}{u(z)\left(\theta(z) - \theta_s\right)} \tag{2.19}$$

Integrating (2.12) and (2.13) with respect to ζ from the roughness height z_0 to a measurement height z gives;

$$\frac{k}{u_*} u(z) = \int_{\zeta_0}^{\zeta} \frac{\phi_M(\zeta)}{\zeta} d\zeta \equiv \Phi_M(\zeta, \zeta_0) \tag{2.20}$$

$$\frac{k}{u_*} (\theta(z) - \theta_s) = \int_{\zeta_0}^{\zeta} \frac{\phi_H(\zeta)}{\zeta} d\zeta \equiv \Phi_H(\zeta, \zeta_0) \tag{2.21}$$

With Eqns. (2.20) and (2.21), Eqns. (2.18) and (2.19) are rewritten;

$$C_D = \frac{k^2}{\Phi_M^2} \tag{2.22}$$

$$C_H = \frac{k^2}{\Phi_M \Phi_H} \tag{2.23}$$

And if we define the bulk Richardson number across the surface to the height z as:

$$Ri_B \equiv \frac{g}{\theta} \frac{z \Delta\theta}{u^2(z)} \tag{2.24}$$

we can write ζ in terms of Ri_B as:

$$\zeta = \beta Ri_B \tag{2.25}$$

where

$$\beta = \frac{\Phi_M^2(\zeta, \zeta_0)}{\Phi_H^2(\zeta, \zeta_0)} \tag{2.26}$$

Hence Eqns. (2.22) and (2.23) can be written in general form, by the use of Eqns. (2.24)-(2.26), as follows:

$$C_D \equiv C^2 f_M(Ri_B, z/z_o) \tag{2.27}$$

$$C_H \equiv \frac{C^2}{r} f_H(Ri_B, z/z_o) \tag{2.28}$$

where $C^2 = [k/\ln(z/z_0)]^2$ is the drag coefficient under neutral conditions and r is a constant. To determine the functional form of f_M and f_H, we used the formulation introduced by Louis (1979) and Louis et.al. (1982) for unstable conditions

$$f_M = 1 - \frac{2b\,Ri_B}{1 + 3abC^2(z/z_o)^{1/2} Ri_B^{1/2}} \tag{2.29}$$

$$f_H = 1 - \frac{3b\,Ri_B}{1 + 3abC^2(z/z_o)^{1/2} Ri_B^{1/2}} \tag{2.30}$$

and for stable conditions

$$f_M = \frac{1}{1 + 2b\,Ri_B(1 + d\,Ri_B)^{-1/2}} \tag{2.31}$$

$$f_H = \frac{1}{1 + 3b\,Ri_B(1 + d\,Ri_B)^{-1/2}} \tag{2.32}$$

where a = b = d = 5.

Above the surface layer, the vertical turbulent fluxes are defined in terms of the eddy diffusivity as:

$$\frac{\tau}{\rho} = \overline{\vec{v}'w'} = -K_M \frac{\partial \vec{V}}{\partial z} \tag{2.33}$$

$$\frac{H}{\rho C_p} = \overline{\theta'w'} = -K_H \frac{\partial \bar{\theta}}{\partial z} \tag{2.34}$$

As in the surface layer, the stratification of the environmental flow should affect the fluxes significantly. One expression of $K_{M,H}$ in terms of wind shear and vertical temperature gradient has the following form (Blackadar, 1979)

$$K_{M,H} = \ell^2 \left| \frac{\partial \vec{V}}{\partial z} \right| f_{M,H}(R_i) \tag{2.35}$$

where ℓ is a mixing length.

The expressions of $f_{M,H}$ in the Eqns. (2.29)-(2.32) were used by Louis (1979) to determine $f_{M,H}$ in Eqn. (2.35), except that Ri_B is replaced by the local Richardson number defined as

$$R_i = \frac{g}{\theta} \frac{\partial \theta}{\partial z} \Big/ \left| \frac{\partial \vec{V}}{\partial z} \right|^2 \tag{2.36}$$

$c^2 (z/z_0)^{1/2}$ in Eqns. (2.29),(2.30) is replaced by

$$\left(\frac{\ell}{\Delta z}\right)^2 \left(\frac{\Delta z}{z}\right)^{1/2} \left[\left(\frac{z+\Delta z}{z} \right)^{1/3} - 1 \right]^{3/2} \tag{2.37}$$

where Δz is the thickness of the model layer. The expression for ℓ suggested by Blackadar (1962) has been used here:

$$\ell = \frac{kz}{1 + kz/\lambda} \tag{2.38}$$

where λ = 150 m for momentum and λ = 450 m for sensible heat (Louis et .al., 1982).

The horizontal turbulent fluxes are defined in terms of the horizontal eddy diffusivity and the horizontal gradient of mean variables:

$$\frac{1}{\rho}\tau_{ij} = -K_m \frac{\partial u_i}{\partial x_j} \tag{2.39}$$

$$\frac{H_i}{\rho C_p} = -K_h \frac{\partial \theta}{\partial x_i} \tag{2.40}$$

where $K_{m,h}$ are horizontal eddy diffusivities of momentum and sensible heat, $\frac{\partial u_i}{\partial x_j}$ is the horizontal gradient of mean flow speed, and $\frac{\partial \theta}{\partial x_i}$ is the horizontal gradient of mean potental temperature. Smagorinsky (1963) has suggested that $K_{m,h}$ be proportional to the magnitude of the horizontal deformation of mean flow. For simulation of three-dimensional turbulence, Lilly (1966) has shown that the formulation of Smagorinsky (1963) for K is consistent with the existence of a three-dimensional inertial subrange on scales comparable to and less than the grid interval. The

suggested by Lilly (1966) is

$$K = (c'\Delta)^2 \, D/\sqrt{2} \tag{2.41}$$

where K is subgrid-scale horizontal eddy diffusivity, Δ is the grid interval, and D is the magnitude of the horizontal deformation of the flow field defined as

$$D = \text{mag}\left[\frac{\partial u_i}{\partial x_j}\left(\frac{\partial u_i}{\partial x_j} + \frac{\partial u_j}{\partial x_i}\right)\right] \tag{2.42}$$

Expanding Eqn. (2.42) for i,j =1,2 and combining with Eqn. (2.41) we have

$$K = \frac{(c'\Delta)^2}{\sqrt{2}}\left[2\left(\frac{\partial u}{\partial x}\right)^2 + 2\left(\frac{\partial v}{\partial y}\right)^2 + \left(\frac{\partial u}{\partial y} + \frac{\partial v}{\partial x}\right)^2\right]^{1/2} \tag{2.43}$$

In our calculation, the horizontal eddy diffusivities for momentum and sensible heat have been set equal to K. Smagorinsky (1963) has used the value c'=.4=k, the von Karman constant, in his numerical calculations of the large scale global atmospheric circulation by setting K and D in Eqn. (2.41) to their respective values within a constant-stress boundary layer,

$$ku_* z_1 = (c'\Delta)\, u_*/kz_1$$

where z_1 is the level of application within the layer.

Solving for c', we have

$$c' = \left(\frac{z_1}{\Delta}\right)k \tag{2.44}$$

If z_1 is comparable to Δ and if the stress within the layer is constant, from Eqn. (2.44), c' = k is appropriate. But one or both of above assumptions is usually violated. Lilly (1966) has estimated c' with the knowledge of the Kolmogorov inertial-subrange constant and suggested c'=.22. In our

calculation, we chose c'=.28. The finite difference form of K given in Deardorff(1970) has been adopted here.

III) Potential-enstrophy conserving finite difference scheme based on a staggered grid

As a finite-difference scheme for the calculation of the advection term, a potential-enstrophy and energy conserving scheme developed by Arakawa and Lamb (1980) has been used. The variables in the horizontal have been staggered using a C grid (Messinger and Arakawa, 1976). The potential-enstrophy and energy conserving scheme was developed to improve the simulation of nonlinear aspects of the flow over steep topography (Arakawa and Lamb, 1980). It was developed and compared to the other potential-enstrophy non-conserving schemes in Arakawa and Lamb (1981). Due to the effect of computational dispersion in the non-conserving scheme, the energy in larger scale motion cascades toward smaller scale motion, and this cascade is almost entirely due to the false computational effects introduced by using the finite-difference form of the continuous equation. Vorticity in atmospheric motion is usually carried by smaller scale motions, hence the effect of computational dispersion usually appears as an increase in the mean potential enstrophy, $\langle \frac{1}{2} \frac{\eta^2}{h} \rangle$, where η is the absolute vorticity, h, a fluid depth and the $\langle\ \rangle$ denotes the domain average. For this kind of problem, a decrease in grid size

can improve the result, but it must be accompanied by a decrease in the time increment. On the other hand, solutions with a scheme that prevents a false energy cascade should be relatively smooth and, therefore, should not be significantly affected by a decrease in grid size. It was pointed out in Arakawa and Lamb (1981) that increasing the order of accuracy does not necessarily guarantee much improvement. If a significant amount of energy is contained in the smallest resolvable scales as a result of spurious energy cascade, convergence of the Taylor expansion of the truncation error may not be fast enough due to the large values of higher-order derivatives. When compared to potential-enstrophy non-conserving schemes, the result of the test presented in Arakawa and Lamb (1981) shows that there was much improvement in the calculation with the coarse grid but not much difference with the fine grid.

The variables in our calculation are ataggered on the C grid. Previous studies (e.g. Messinger and Arakawa) have shown the superiority of the staggered grid over the non-staggered grid. The performance of various grids, staggered or non-staggered, has been well summarized in Messinger and Arakawa (1976). They considered the group velocity of inertia-gravity waves to be a monotonically increasing function of wave number, and selected the C and B grids as those which performed best. Defining the Rossby radius of deformation as $\lambda \equiv \frac{\sqrt{gH}}{f}$

and the grid spacing as D, Arakawa and Lamb (1976) showed that for $(\lambda/D)>1$, the group velocity has the wrong sign with the B grid while it remains correct with the C grid regardless of the grid spacing. For typical atmospheric mesoscale problems, where λ is of order 1000 km and D of order 100 km or less, the C grid was shown to be superior to the other grids. But because two velocity components are carried at different positions in space in the C grid, there are difficulties in calculating the Coriolis-force term. A further important problem with the C grid is that the group velocity of the shortest resolvable wave (2Δ wave) becomes zero, and hence there is not dispersion of wave energy for the shortest resolvable wave. This causes two-grid-interval noise that was stationary as a pure gravity wave, and behaves like a pure inertial oscillation. This two-grid-interval noise was partially removed by inclusion of the horizontal diffusion term.

2-2 Experimental Design

In order to simulate the effects of isolated topography on th flow field, Oahu island and the surrounding ocean area of 130 km x 100 km were chosen as the model orography. The use of real-world island orography in the model is primarily useful to verify the model results against actual observations. On the other hand, the detailed effects of the topographic barrier are difficult to investigate due to the complexity of the island topography. The model domain was covered with a 5 km x 5 km grid mesh of 26 x 20 grid points in the horizontal and with seven irregularly spaced layers in the vertical. The irregularly spaced vertical coordinate was chosen in order to give finer resolution to lower layers where most of the disturbances of interest take place. The vertical spacing between the layers ranges from 100 m for the lowest layer to 2.6 km for the uppermost layer. The height of the island was digitized by hand from the map of Oahu island, and was subjectively smoothed in order to represent the area averaged value within each grid box. This procedure removed local extremes.

Ground and ocean surfaces have considerably different responses to solar heating. In order to take these different responses into account, the sea-surface temperature was held fixed while the ground-surface temperature was diagnosed by an energy balance equation (Deardorff, 1978). In addition, different roughness lengths over the ocean and ground surface were used to

represent the different frictional characteristics of different surfaces. The roughness lengths used are:

z_0=.4 m for land surface higher than 150m

z_0=.25 m for land surface lower than 150m

z_0=.001m for ocean surface. Two different values of z_0 were used on the land in order to distinguish the shore regions, where intermediate surface friction is expected, from the mountainous areas.

The large-scale flow was taken as east-north-easterly, and was assumed to be constant inside the domain. Also, the large-scale flow was assumed to be in geostrophic balance with the large-scale pressure field. The values used for large-scale flow are:

Ug =-6.9 m/sec

Vg =-1.9 m/sec

This geostrophic flow field given above was used to calculate the forcing due to the large scale pressure gradient.

As an initial wind field, an Ekman balanced flow in the lowest three layers was assumed with respect to a flat surface according to given roughness lengths over the ground and the ocean surface.

The specified day was a sunny day of June 21 of arbitrary year, and the model atmosphere was assumed to contain no moisture, for simplicitly.

The ground-surface potential temperature on the flat surface was initially set 2°K lower than that of the lowest-layer potential

temperature and was set equal to the lowest-layer potential temperature at the sea surface. At time t =0 (0100 LST), the island was caused to begin growing from a flat bottom, and the ground surface potential temperature was adjusted with an assumed lapse rate of 2°K/km to give lower potential temperature in the valleys. The initial potential temperature distribution of the model atmosphere was given to be constant up to about 700m (lowest three layers) and to increase continuously aloft. The initial stratification between the layers, in terms of Brunt-Vaaisalla frequency $N^2 = \frac{g}{\theta}\frac{d\theta}{dz}$, and vertical spacing of sigma surfaces are shown in Fig. (2.1).

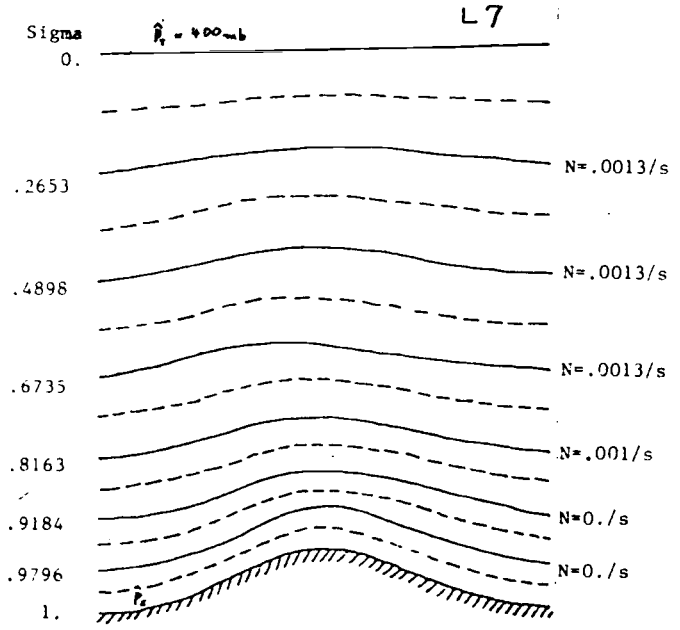

Fig. 2.1 Vertical spacing of sigma surfaces and initial stratification

As the lateral boundary condition, a cyclic condition was imposed. The solid-surface upper and lower boundary condition (zero transverse flow) was used during the model calculation. A time step of 5 s was used to advance the dependent variables. For the adiabatic experiment, the same conditions described above were implemented, but without vertical heat flux between the model atmosphere and underlying topographic surface.

CHAPTER 3

Results of the Numerical Experiments

The numerical integrations were carried out for sixteen hours beginning from 0100 LST.

The descriptions of the results will be made on const-sigma surfaces unless it is necessary to express them in the p- or z-coordiante system. This is in order to avoid errors which may be involved in vertical interpolation or extrapolation procedures.

Vertical cross-sections of the resulting flow field are constructed along the line CC in Fig. (3.3). In order to construct the vertical cross-sections, horizontal and vertical velocities, as well as potential temperature, were assumed to vary linearly with respect to the geopotential height between the two reference levels on which those variables are defined.

Detailed descriptions and analyses of the experimental results will be given in the following sections.

3-1 The Sea-level Pressure Perturbation and Associated Low-level Flow Field

An asymmetric pressure perturbation and lateral deflection of the low level streamlines at the upwind side of a topographic obstacle appear in observations and in studies using linear and nonlinear models. Pierrehumbert and Wyman (1985) show the splitting of low level flow observed during the ALPEX. In the same

work they also show, by a scale analysis and simple nonlinear model, that the pressure perturbation at the upslope of a mountain would be enough to have an O(1) decelerating effect on the incoming flow when the inverse of the Froude number, Nh/U, becomes unity, where h is the height of the topographic barrier.

In the presence of a three-dimensional topography and a stable stratification in the vertical, the upstream blocking by the topographic barrier would not be so strong as in a two-dimensional case because of the lateral dispersion arising from the three-dimensionality. Smith (1980) has shown in his linear study that for a steady flow of vertically unbounded, hydrostatic, stably stratified Boussinesq flow, over small amplitude topography with negligible effect of the earth's rotation, lateral deflection of incoming flow takes place at the upwind side of an isolated, bell-shaped mountain.

Even though the above studies give qualitatively correct explanations of the effect of irregular terrain, thermal forcing by a heated ground surface during daytime is also important in determining the flow field near a topographic barrier. Especially when land-sea contrast exists, the effect of the insolation and temperature advection will be shown to be of great importance in the resulting daytime flow field.

Figs. (3.1) and (3.2) show the sea-level pressure perturbation. To reduce the ground-surface pressure to sea-level,

the "atmosphere" under the ground-surface was assumed to be isentropic. Although an isothermal atmosphere under the ground-surface is usually assumed in order to reduce the ground-surface pressure to sea-level, the results from both assumptions showed very little difference for our case. An isentropic assumption was chosen for the convenience of the calculation. In the morning when insolation is weak, high sea-level pressure appears at the upslope of the island and low pressure appears at the lee side. Linear studies (Queney, 1948; Smith, 1981) have shown that when the Froude number is large, a vertical displacement of the streamlines is possible, causing an asymmetric pressure field with high pressure at the upslope and low pressure at the downslope of a topographic barrier. The above studies also predict that maximum lifting of streamlines would take place at the upslope of the topography, not at the top of it. Setting N=.01/s, U=10m/s and h=600m, the Froude number, U/Nh, of the model atmosphere in the early morning is greater than 1. Hence we expect the large Froude-number theory would be valid before the heating of the island surface becomes important. In other words, without the effect of diabatic heating, the flow field is governed by the pressure perturbation generated by the topographic slopes. As solar heating of the island surface becomes strong, the sea-level pressure perturbations show an appreciable change. The peak of high presure at the upslope

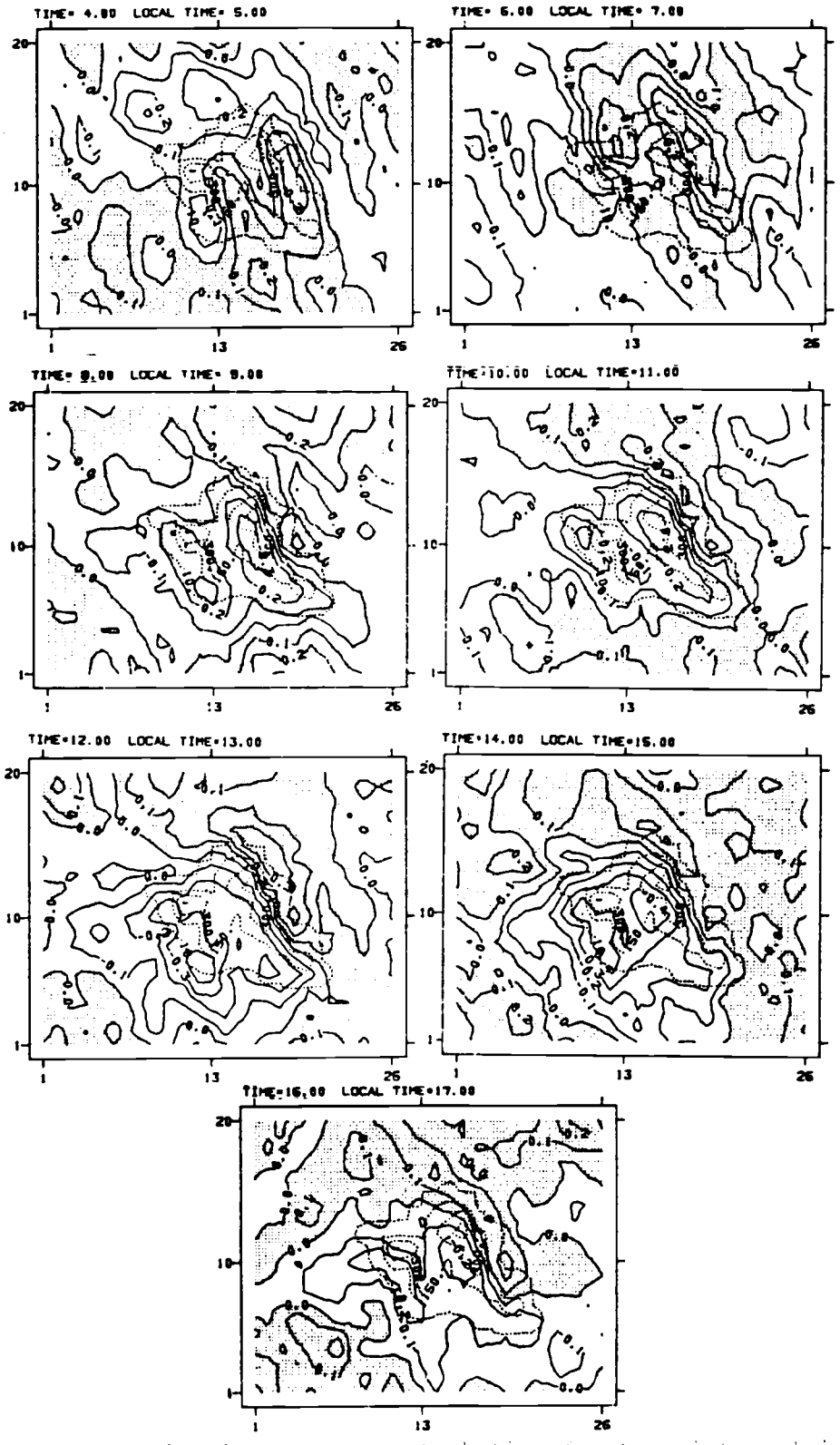

Fig. 5.1 Sea-level pressure perturbation (contour interval is ... mb; one grid interval is 5km)

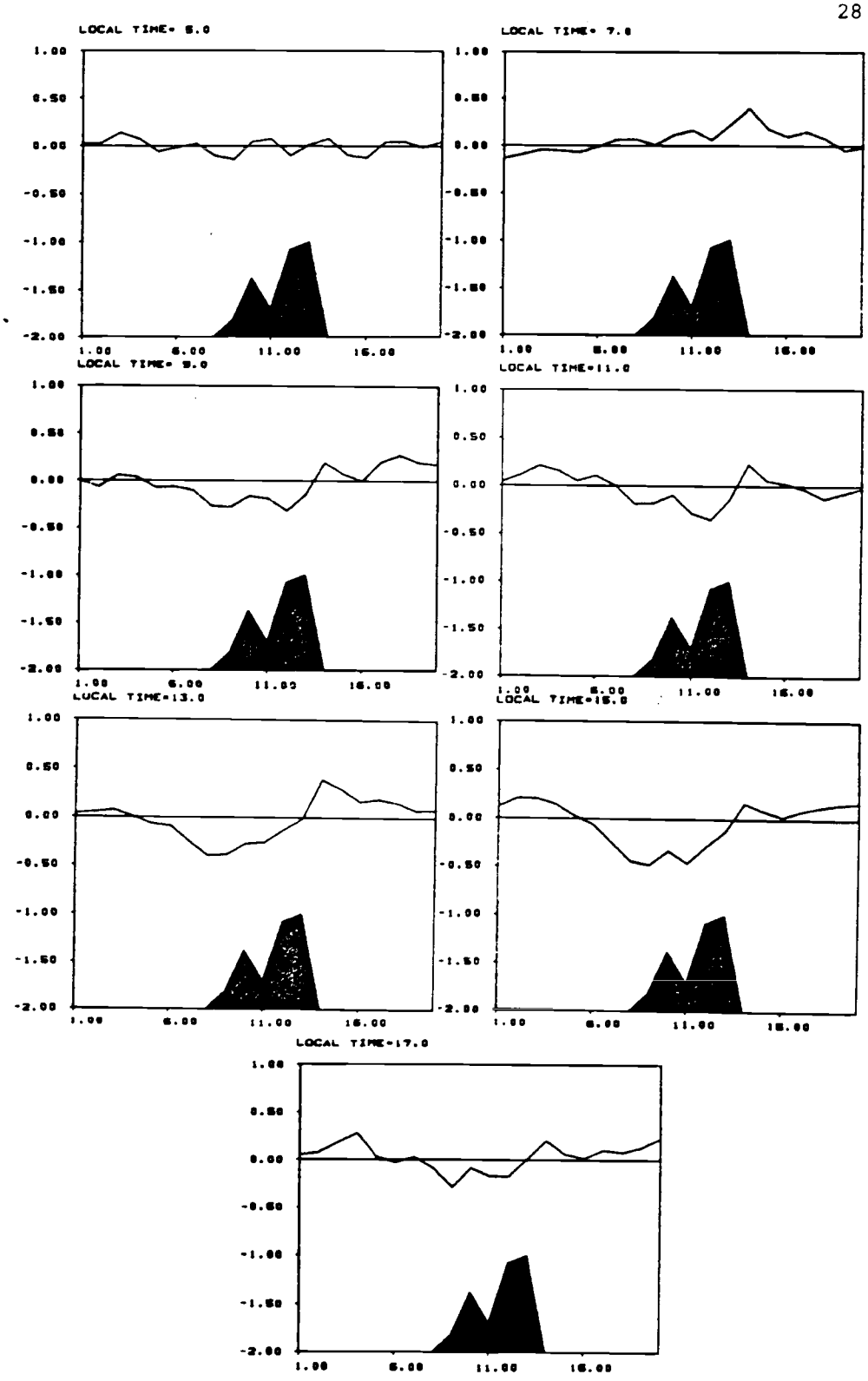

Fig. 3.2 Sea-level pressure perturbation along the line CC in Fig. 3.3 one unit of abscissa is 7.7km and the unit of ordinate is mb.

persists, and the low pressure at the lee side of the island deepens significantly. Low pressure develops at the inland portion of the island where high pressure had occurred during the early morning. These effects of ground heating appear to be important for the daytime flow field, and will be discussed in detail in the following sections.

Fig. (3.4) shows the divergence of horizontal velocity components. This divergence closely resembles to that of horizontal mass divergence in its locations and sign.

The asymmetry of the sea-level pressure perturbation and its diurnal variations are very well reflected in the low level wind and divergence fields (Figs. (3.3) and (3.4)).

Lateral deflection of the streamlines associated with the high pressure at the upwind side and the horizontal convergence induced by the low pressure at the lee side of the island are clearly seen in the above fields. It is also shown in Fig. (3.2) that the pressure gradient opposes incoming flow at the upwind side of the island. Pierrehumbert and Wyman (1985) have shown that for a two-dimensional ridge, the pressure perturbation caused by the lifting of low-level dense air by the upslope of the ridge, slows down the incoming flow and its influence can reach far upstream. Unlike a two-dimensional case, the flow is only partly blocked by a three-dimensional mountain, and the effect of the blocking is confined to the vicinity of the mountain.

With an increase of daytime heating of the island surface, a slight tendency can perhaps be seen from Fig. (3.3) for the flow to tend to split into streams more parallel to the mountain range at the upwind side of the island. This tendency also appears in the numerical simulation over a meso-scale mountain presented by Mahrer and Pielke (1977). But no proper explanation for this result can be made at the present stage and further study is needed. The low pressure over the island induces more flow toward the island. Especially at the lee side, the direction of the low-level flow is reversed, showing a well defined sea-breeze regime.

The horizontal-divergence field appears to be consistant with the pressure fluctuations forced by the topographic slopes and daytime heating. At the windward side of the island, the horizontal divergence is only a little affected by daytime heating. The strongest convergence arises at the shore region, A, where the pressure-gradient force opposing the incoming flow is large. And the region of divergence at the upslope of the island, B, appears to be related to the lateral deflection of low-level flow. A divergence appearing at the mountain top, C, is again associated with the pressure- gradient force acting to accelerate the mean flow.

Unlike at the upwind side, horizontal divergence at the lee side of the island undergoes large diurnal variations. With

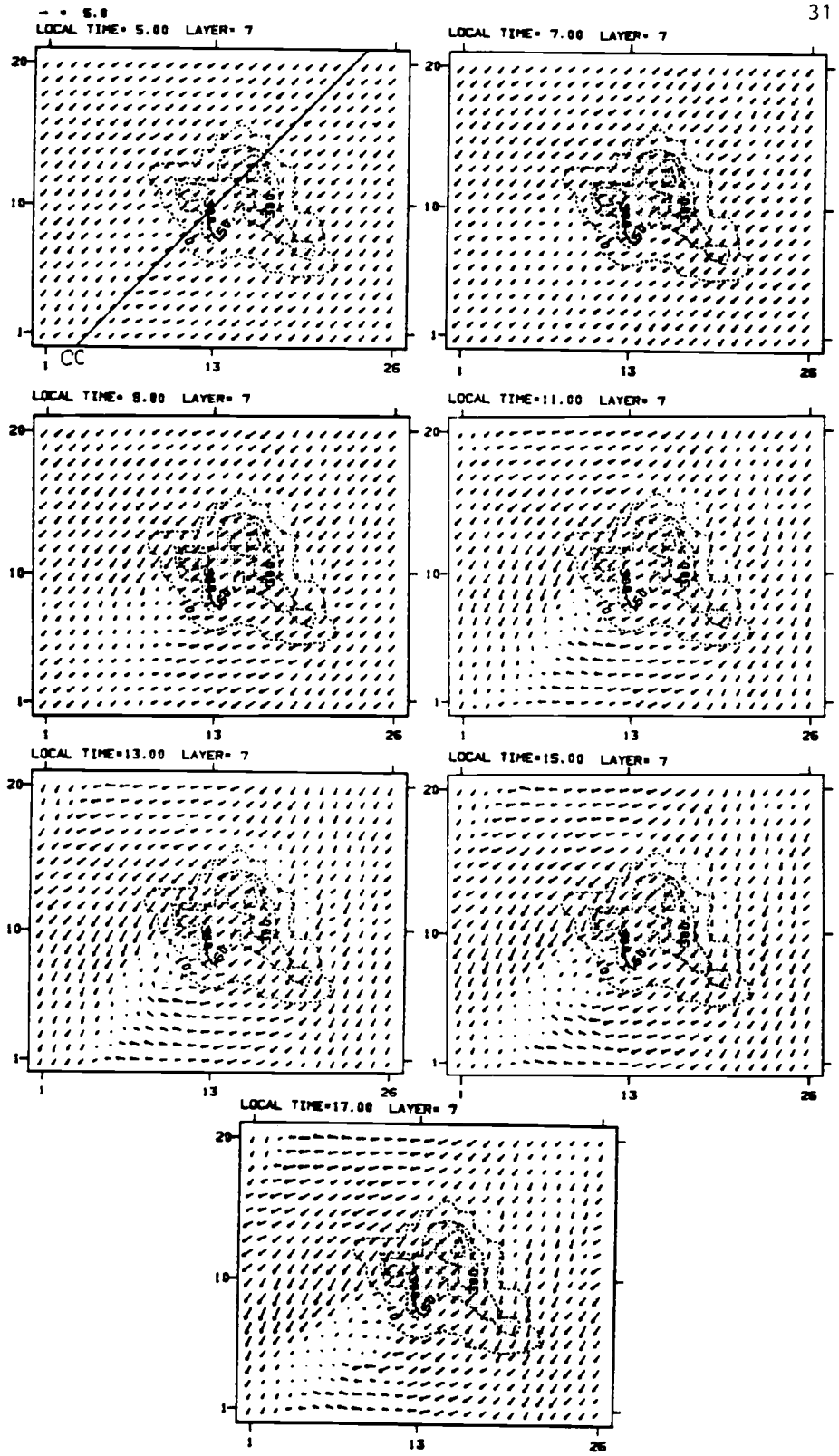

Fig. 3.3 Horizontal wind field in the lowest layer.

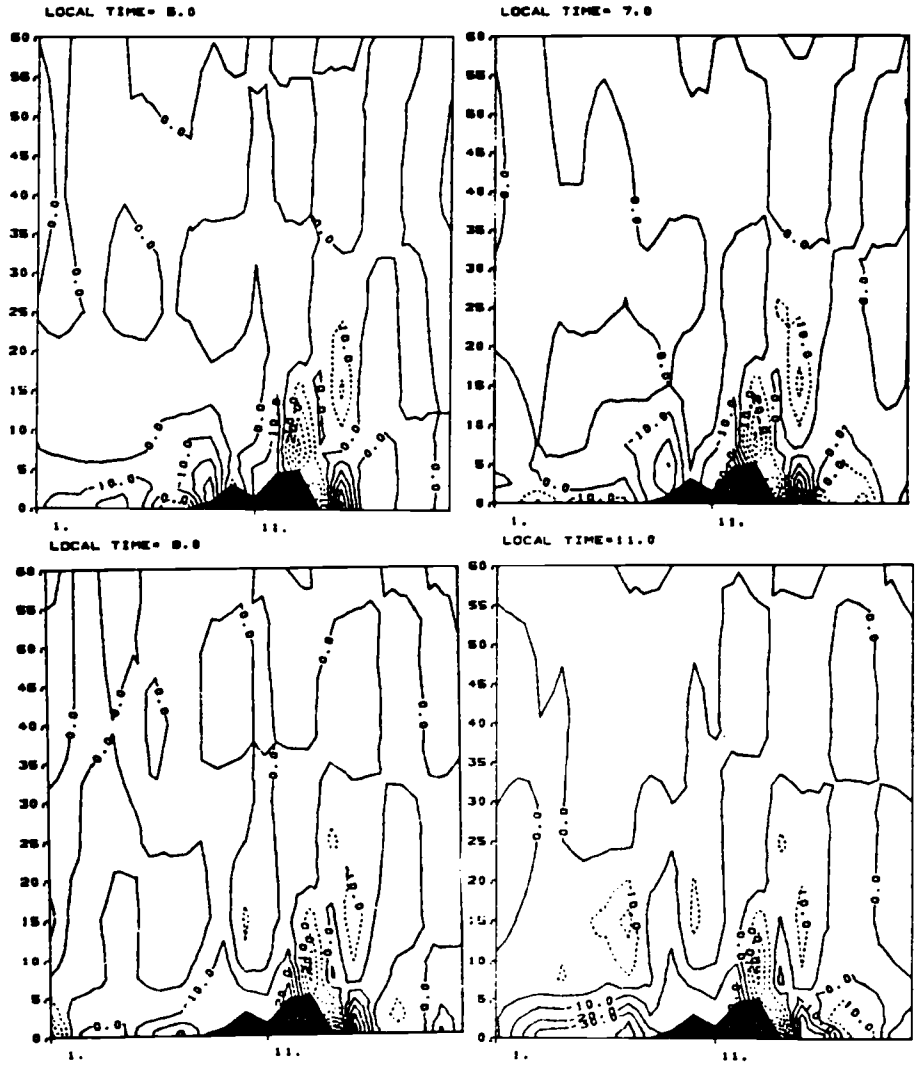

Fig. 3.4 Vertical cross-section of $\nabla_H \cdot V_H$ along the line CC in Fig. 3.3 (contour interval is .0001/s and the units of the abscissa is 100m).

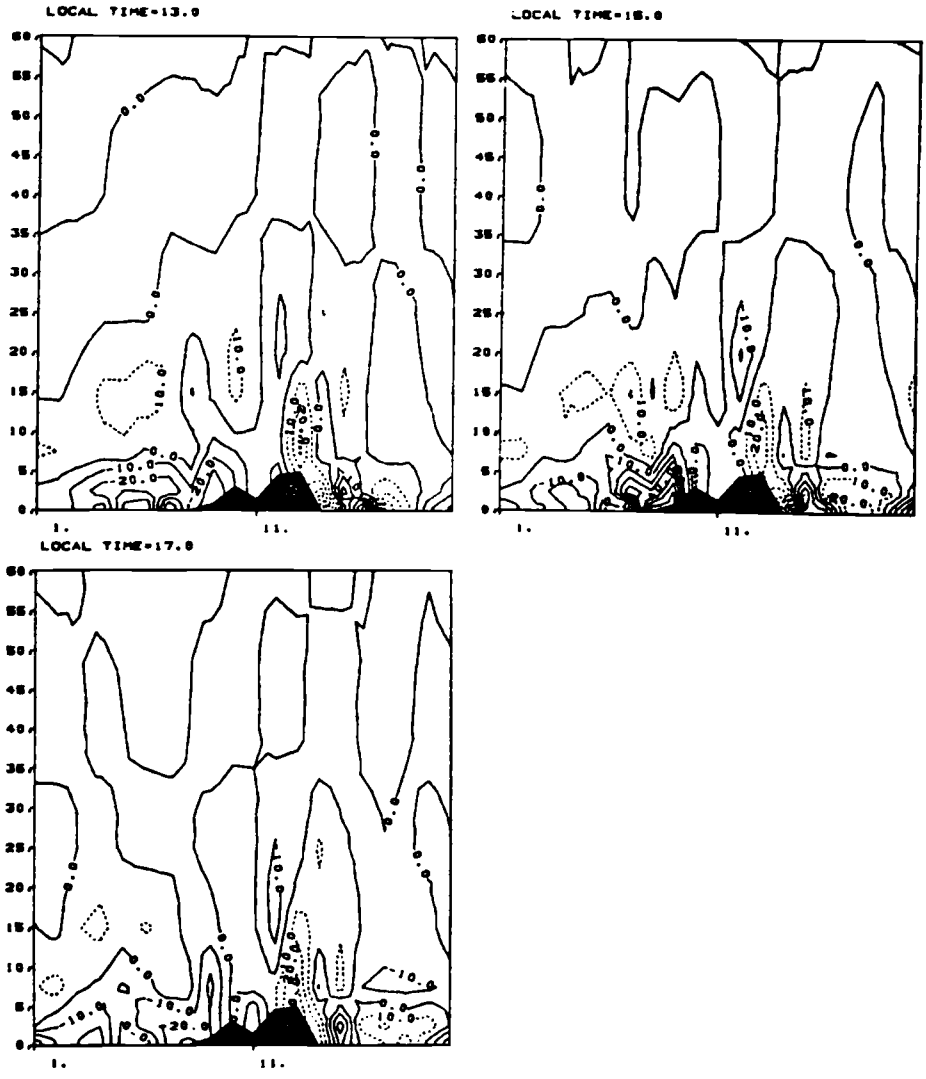

Fig. 3.4 (continued)

intense solar heating, the convergence at the lee side of the island is further intensified. This intensified convergence is the consequence of deepening of the low pressure at the lee side of the island.

Near the ground surface, the vertical motion is determined by the kinematic boundary condition, hence rising motion occurs along

upslopes and sinking motion along downslopes.

But above the ground surface, the vertical motion is strongly related to the horizontal mass-divergence field associated with the pressure fluctuations. Comparing the vertical motion and vertical distribution of the horizontal divergence fields, it is clear that the vertical motion over the ocean, where topographic slopes are absent, is entirely determined by the horizontal divergence field.

Over the island, vertical motion is strongly affected by the topographic slopes, especially near the topographic surfaces. As an example, rising motion at the mountain top, C, appears between the low-level divergence and upper-level convergence. This vertical distribution of divergence fields, through the mass continuity, tends to cause sinking motion between those levels. But the rising motion forced by the upslope, which appears as a lower boundary condition, can overcome this effect and still prevails there.

As daytime solar heating increases, rising motion over the island becomes strong following the increased horizontal convergence (or weakened horizontal divergence). At the lee slope of the island, sinking motion related to the downslope is confined to the low level just above the topography, and rising motion associated with the increased low-level convergence takes place aloft.

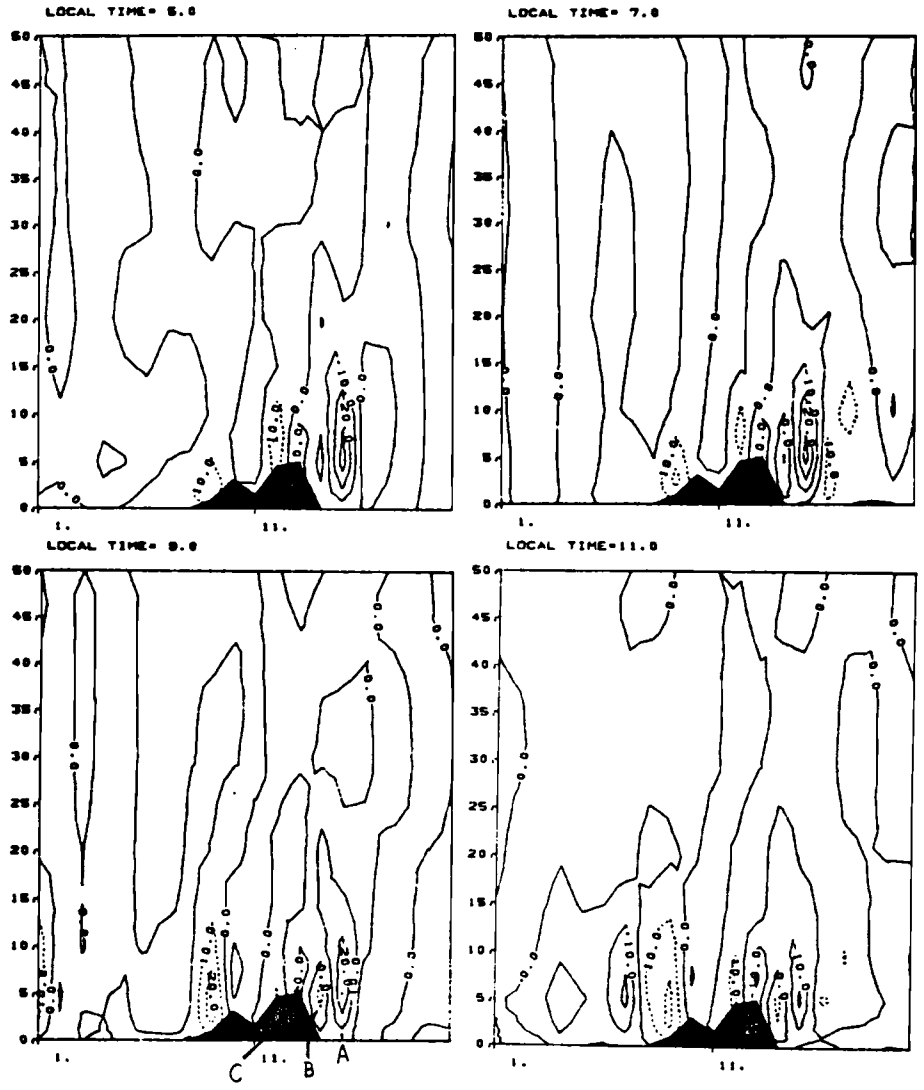

Fig. 3.5 Vertical cross-section of p-velocity along the line CC in Fig. (3.3) (contour interval is .01 mb/sec and the units of the abscissa is 100m).

3-2 The Effects of the Heating of the Island Surface

The effect of the heating of the ground surface, whose time scale is less than a day, is usually confined to the lower atmosphere unless condensation takes place aloft. In the presence

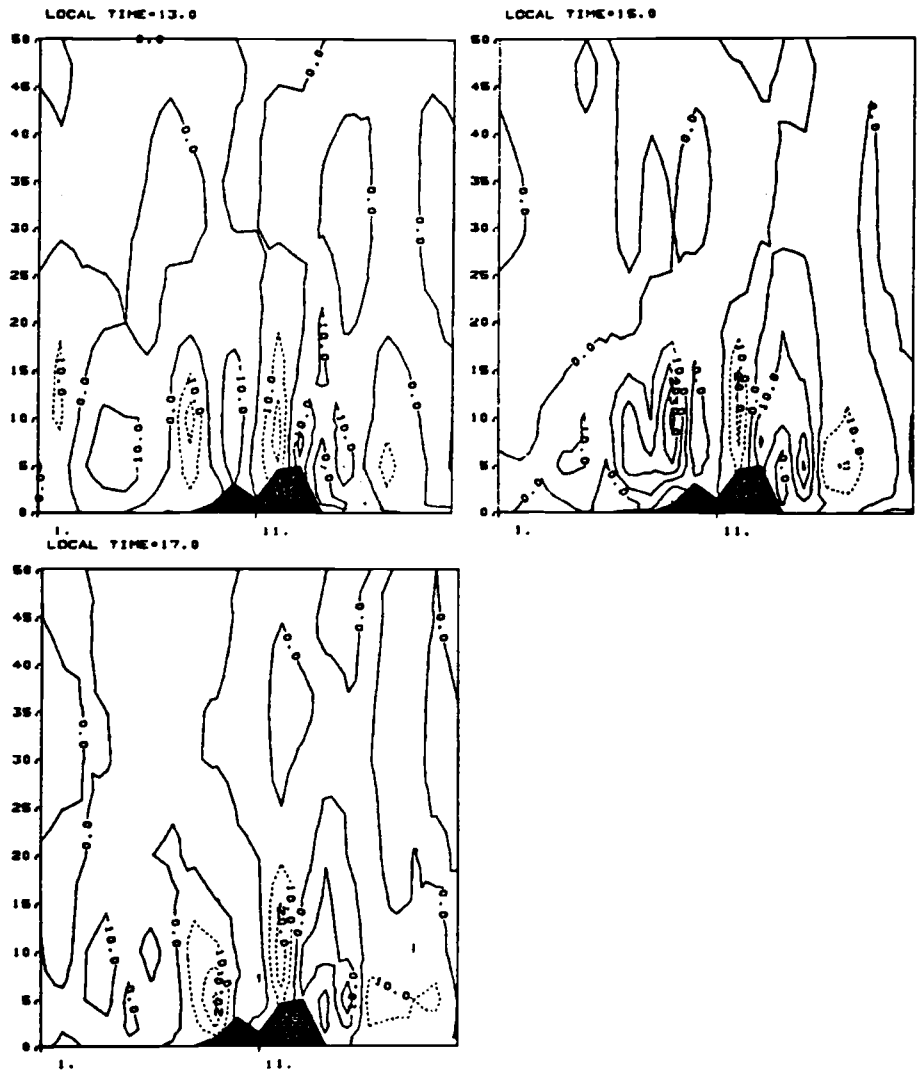

Fig. 3.5 (continued)

of a land-sea contrast, different responses of the underlying surfaces to insolation lead inhomogeneous mixed-layer temperature and depths over the underlying surfaces. With the assumption that the upper troposphere is relatively unaffected by the heating of time scale less than a day, a hydrostatic relationship predicts a

lower sea-level pressure for a higher vertically-integrated mixed-layer temperature.

Fig. (3.6) shows a vertical cross-section of potential temperature and Fig. (3.7) shows vertical profiles of potential temperature at 1500 LST over three different points P1,P2, and P3, along the mean flow direction. The most distinct features of these figures are the increase of the depth and potential temperature of the mixed layer over the island along the direction of the mean flow. The mixed-layer potential temperature changes according to the sensible heat flux from the underlying surface, entrainment of the ambient air at the top of the mixed layer, and horizontal temperature advection by the mean and perturbation flow. During daytime the mixed-layer temperature over the island is higher than over the ocean due to the higher surface temperature at the island. At the windward side of the island, the temperature advection by the mean flow is from the ocean surface. This advection of cool air tends to reduce the low-level potential temperature at the upwind side of the island. The mountain range at the upwind edge of the island partly blocks the low-level cool air and prevents it from penetrating further inland. Also, the low-level flow is gradually heated while passing over the island surface.

Hence the cooling due to cold-air advection decreases downstream over the island, resulting in the warmer mixed layer at the inland and lee side of the island.

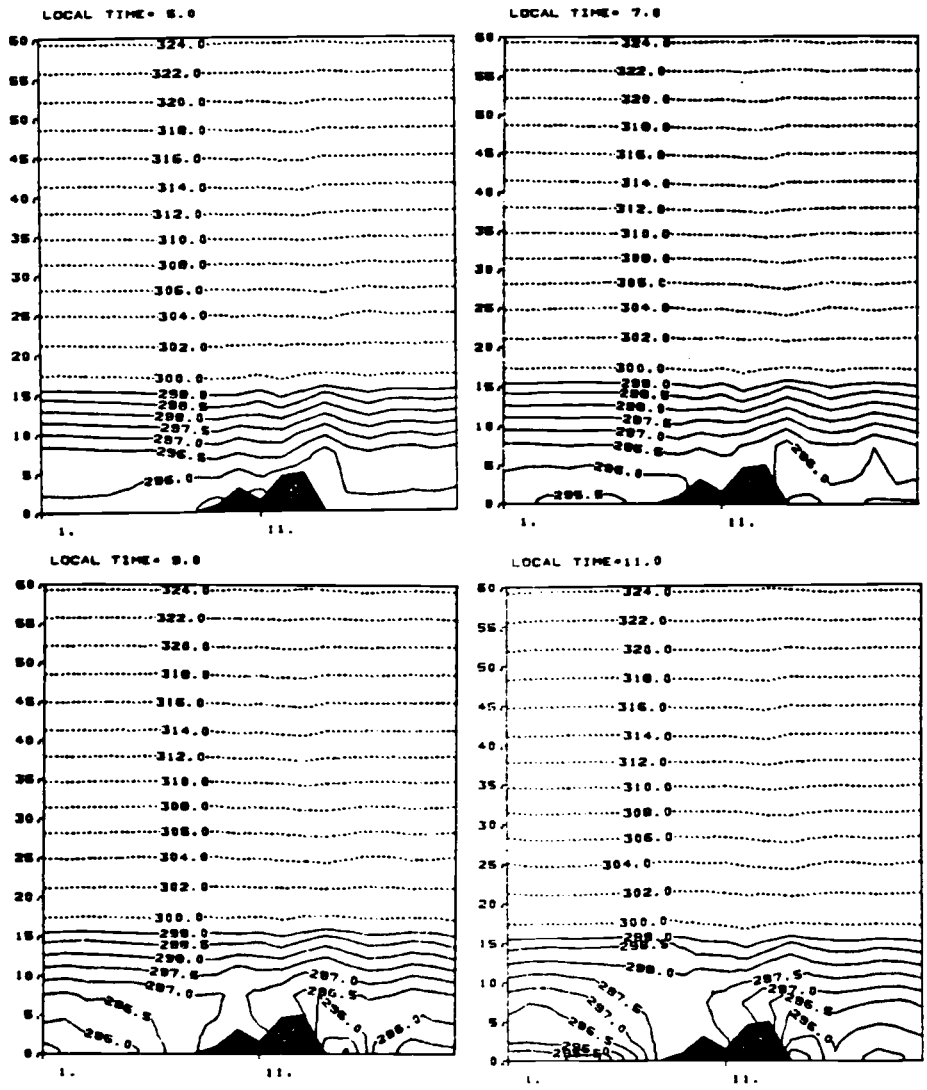

Fig. 3.6 Vertical cross-section of potential temperature along the line CC in Fig. 3.3

As we have seen above, horizontal divergence and associated vertical velocities are significantly affected by the daytime heating, especially at the lee side of the island. This thermal forcing is strong enough to break down the lee side wave structure generated by the orographic forcing in the morning. But the wave motion at the upwind side of the island appears to be only a

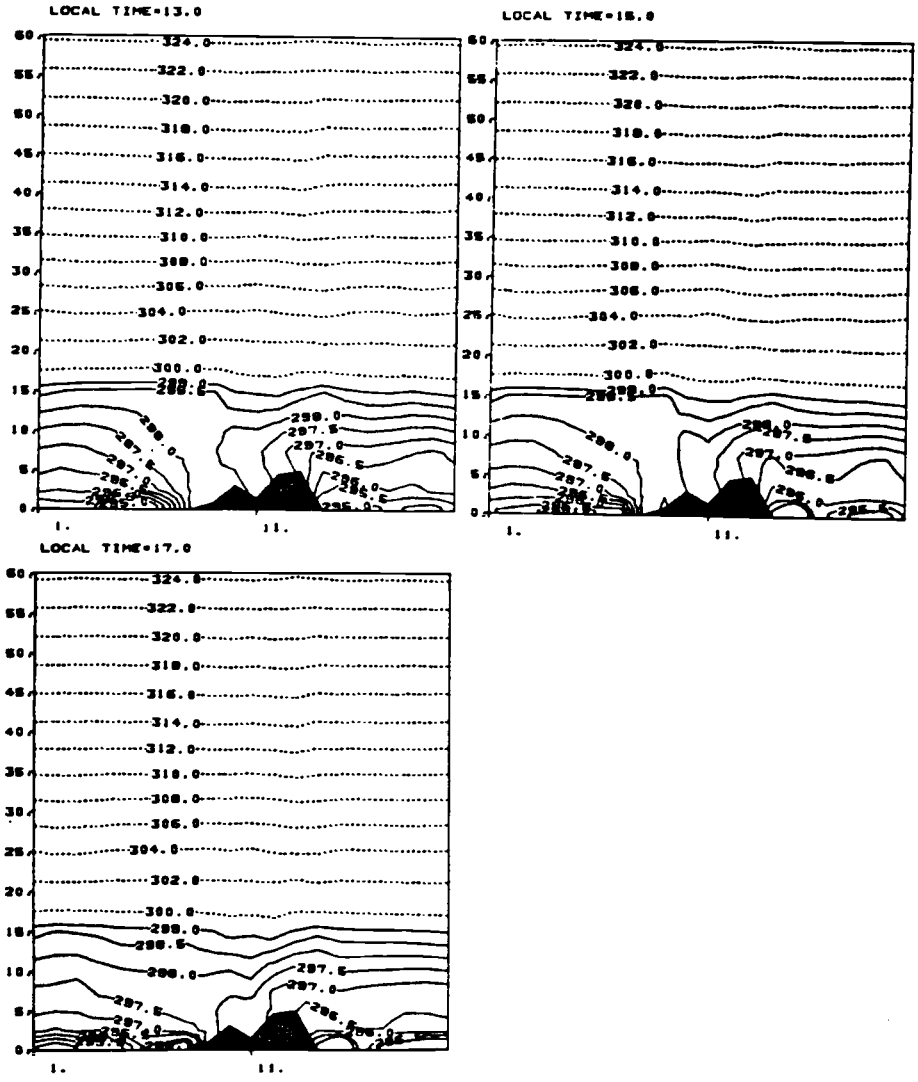

Fig. 3.6 (continued)

little affected by the thermal forcing. The over-all steadiness of the flow field at the upwind side of the island re-emphasizes the importance of the topographic blocking in determining the flow field at the upwind side. And the large diurnal variation of the flow field at the lee side of the island suggests that the effect

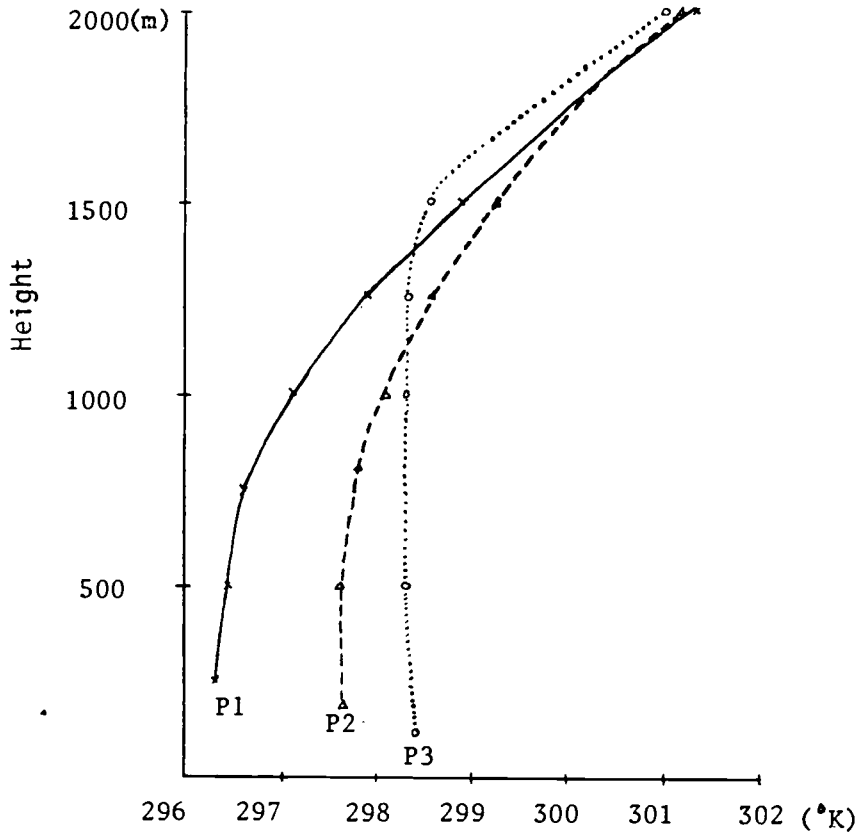

Fig. 3.7 Vertical profile of potential temperature at the points P1, P2, and P3 at 13:00 LST.

of the daytime heating is significant at the lee side where the pressure perturbation by the topographic effect and by the thermal effect are in phase, and where the cooling by temperature advection is small.

3-3 Hydrostatic Mountain Waves Generated by the Island Topography

In the earlier sections, we briefly mentioned the wave-like motions appearing in the vertical velocity and horizontal divergence fields. A well defined wave motion takes place over the island, and the waves over the ocean surface appear with reduced magnitudes.

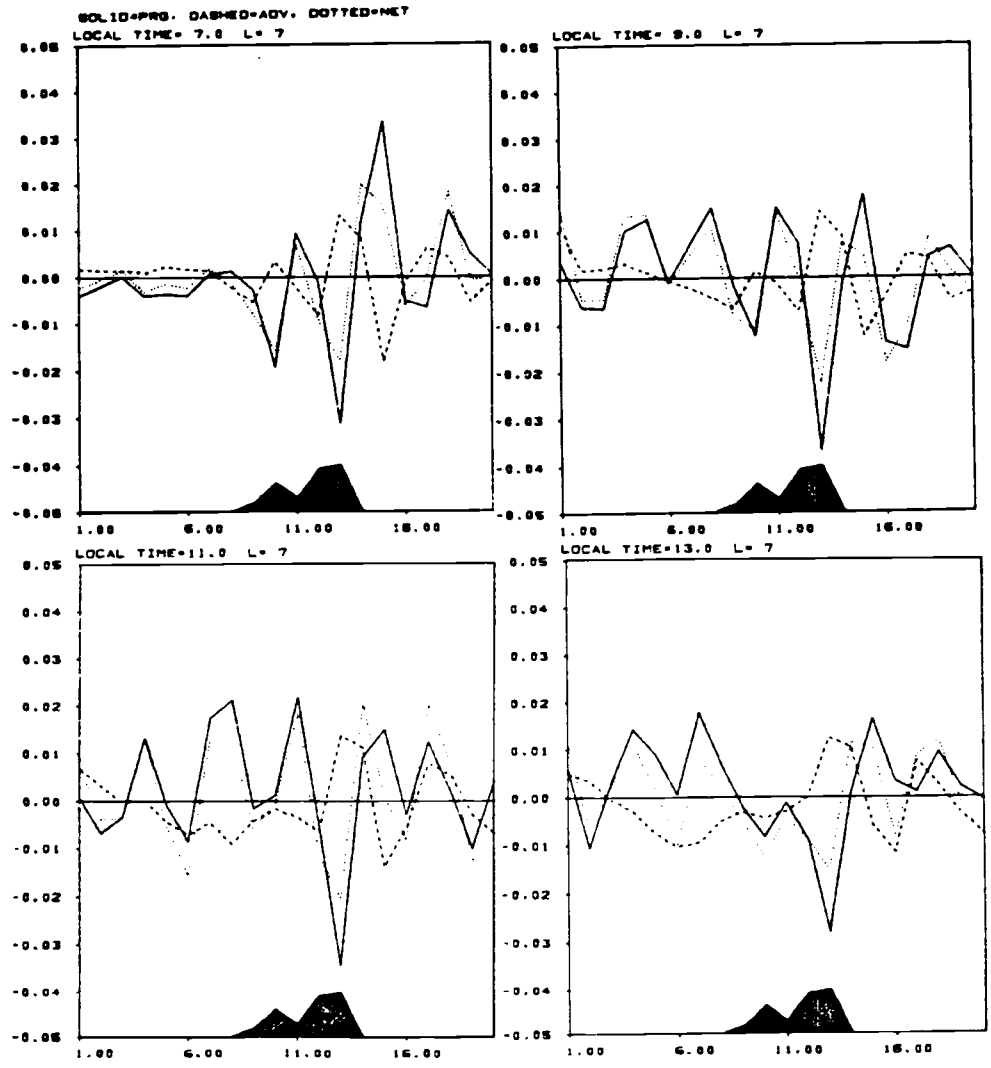

Fig. 3.8 Forcing due to horizontal pressure gradient (solid line), advective acceleration (dashed line) and sum of both (dotted line) in the lowest layer along the line CC in Fig. 3.3. (Ordinate scale is m/s^2)

Before we begin to discuss the results of the numerical experiment, it will be helpful to review the previous studies of this problem with linear models. It should be pointed out that a good summery of early works has been presented in Queney (1948), and the studies to be reviewed hereafter are essentially the three-dimensional versions of Queney's second problem.

Wurtele (1957) has considered the waves forced by a plateau of cross-stream width 2b, height h, and semi-infinite in the downstream direction. By assuming incompressibility and negligible Coriolis effect, he found that the resulting disturbances are composed of waves whose tilt of wave crests and amplitudes decrease downstream. His results are valid only far downstream, and describe the nonhydrostatic dispersive tails (Smith, 1980).

Smith (1980) has considered the perturbation by a bell-shaped, three-dimensional mountain profile. The following discussions are basically based on his study.

Let us consider a hydrostatic, incompressible Boussinesq flow over a small amplitude topography with negligible effect of the earth's rotation. A hytrostatic assumption can be valid when the advective time scale, a/U, is greater than the buoyancy time scale, $1/N$, where a is the half width of the mountain profile. For the present model parameters, a must be larger than 1km. The length scales of the present study, which are taken to be the half widths of the ridges, are of order 10 km, hence the hydrostatic

assumption can be justified. With the above assumptions, the governing equations are

$$\rho_0 (u_t + U u_x) = - p_x \tag{3.1a}$$

$$\rho_0 (v_t + U v_x) = - p_y \tag{3.1b}$$

$$0 = - p_z - \rho g \tag{3.1c}$$

$$u_x + v_y + w_z = 0 \tag{3.1d}$$

$$\rho = - \frac{d\bar{\rho}}{dz} \eta \tag{3.1e}$$

where x,y,z are the downstream, cross-stream and vertical coordinates; u, v, w, ρ, η, p are the corresponding perturbation velocity components, density, vertical displacement and pressure; and U, ρ, $d\bar{\rho}/dz$ are the bakcground mean wind speed, density, and vertical density gradient which are taken to be constants over the entire domain, and the subscripts denote the partial differentials. Following the kinematic condition

$$w = \eta_t + U \eta_x \tag{3.2}$$

the system (3.1) with Eqn. (3.2) can be reduced to a single equation for $\eta(x,y,z,t)$

$$\eta_{tzz} + 2U \eta_{txz} + U^2 \eta_{xxzz} + N^2 (\eta_{xx} + \eta_{yy}) = 0 \tag{3.3}$$

where $-N^2 = (g/\bar{\rho})(d\bar{\rho}/dz)$ is taken to be a constant. Assuming a wave solution for $\eta(x,y,z,t)$

$$\eta(x,y,z,t) = \iiint_{-\infty}^{\infty} \tilde{\eta}(k,l,m,\sigma)\, e^{i(kx+ly+mz-\sigma t)}\, dk\,dl\,dm\,d\sigma \tag{3.4}$$

we have the dispersion relation

$$\sigma = Uk \pm \frac{N}{m}(k^2+l^2)^{1/2} \tag{3.5}$$

where k, l, m, σ are the downstream, cross-stream, and vertical wave numbers, and the frequency of the wave, respectively. From the dispersion relation we can get the phase and group velocities, C_p and C_g

$$C_{px} = \frac{\sigma}{k} = U \pm \frac{N}{mk}(k^2+l^2)^{1/2} \tag{3.6a}$$

$$C_{py} = \frac{\sigma}{l} = U\frac{k}{l} \pm \frac{N}{ml}(k^2+l^2)^{1/2} \tag{3.6b}$$

$$C_{pz} = \frac{\sigma}{m} = U\frac{k}{m} \pm \frac{N}{m^2}(k^2+l^2)^{1/2} \tag{3.6c}$$

$$C_{gx} = \sigma_k = U \pm \frac{kN}{m}(k^2+l^2)^{-1/2} \tag{3.6d}$$

$$C_{gy} = \sigma_l = \pm \frac{lN}{m}(k^2+l^2)^{-1/2} \tag{3.6e}$$

$$C_{gz} = \sigma_m = \mp \frac{N}{m^2}(k^2+l^2)^{1/2} \tag{3.6f}$$

There is no source of wave energy aloft, hence, the wave energy must propagate upwards. With this condition, for m>0, positive C_g is required. Hence we have

$$\sigma = Uk - \frac{N}{m}(k^2+l^2)^{1/2}$$

Then Eqns. (3.6) become

$$C_{px} = U - \frac{N}{mk}(k^2+l^2)^{1/2} \tag{3.7a}$$

$$C_{py} = U\frac{k}{l} - \frac{N}{ml}(k^2+l^2)^{1/2} \tag{3.7b}$$

$$c_{pz} = U\frac{k}{m} - \frac{N}{m^2}(k^2+\ell^2)^{1/2} \tag{3.7c}$$

$$c_{gx} = U - \frac{kN}{m}(k^2+\ell^2)^{-1/2} \tag{3.7d}$$

$$c_{gy} = -\frac{\ell N}{m}(k^2+\ell^2)^{-1/2} \tag{3.7e}$$

$$c_{gz} = \frac{N}{m^2}(k^2+\ell^2)^{1/2} \tag{3.7f}$$

For a stationary wave, $\sigma = 0$, hence

$$m = \frac{N}{U}\frac{(k^2+\ell^2)^{1/2}}{k} \tag{3.8}$$

In order to be stationary, with N>0 (stable stratification), m must be chosen to have the same sign as k (Eqn. 3.7a). This choice of m and k also implies a windward tilt of the phase line. With this choice of m, the group velocities of the stationary wave are

$$c_{gx} = \frac{U\ell^2}{k^2+\ell^2} \tag{3.9a}$$

$$c_{gy} = -\frac{Uk\ell}{k^2+\ell^2} \tag{3.9b}$$

$$c_{gz} = \frac{U^2k^2}{N(k^2+\ell^2)^{1/2}} \tag{3.9c}$$

The above Eqns. (3.9) imply that the wave energy propagates upwards, downstream as well as laterally. By assuming a steady state, Eqn. (3.3) is rewritten

$$\eta_{xxzz} + \frac{N^2}{U^2}(\eta_{xx} + \eta_{yy}) = 0 \tag{3.10}$$

To obtain a solution to (3.10) we express η as a double Fourier integral

$$\eta(x,y,z) = \iint_{-\infty}^{\infty} \hat{\eta}(k,l,z)\, e^{i(kx+ly)}\, dk\,dl \tag{3.11}$$

With the above expression of η, (3.10) becomes

$$\hat{\eta}_{zz} + m^2 \hat{\eta} = 0 \tag{3.11}$$

where m is given in (3.8). The solution to (3.11) is

$$\hat{\eta}(k,l,z) = \hat{\eta}(k,l,0)\, e^{imz} \tag{3.12}$$

As was shown earlier, m and k must have the same sign. At z = 0, the streamline is assumed to follow the topographic contour, hence the linearized boundary condition

$$\hat{\eta}(k,l,0) = \frac{1}{4\pi^2} \iint_{-\infty}^{\infty} h(x,y)\, e^{-i(kx+ly)}\, dx\,dy$$

where h(x,y) is the bottom topography. Then is finally given by,

$$\eta(x,y,z) = \iint_{-\infty}^{\infty} \hat{\eta}(k,l,0)\, e^{imz}\, e^{i(kx+ly)}\, dk\,dl \tag{3.13}$$

The above integration is not easy to evaluate for arbitrary ground topography. By assuming a bell-shaped mountain profile, Smith (1980) has shown that the pressure perturbation at the surface is

$$p(x,y,0) = -\rho_0 U N h\, \frac{x/a}{(1 + r^2/a^2)^{3/2}} \tag{3.14}$$

where $r^2 = x^2 + y^2$, and the mountain top is located at x=y=0. From (3.14), the maximum surface-pressure perturbations along the

line y=0 arise at $x=\pm a/\sqrt{2}$, with high pressure at the windward slope and low pressure at the lee slope. This peak of high pressure is evident in Fig. (3.1). The peak of low pressure at the lee slope is not quite clear in that figure, but the minor depressions at the lee slopes can be interpreted as the consequence of the pressure perturbations induced by the topographic slope. The pronounced daytime peak of low pressure at the lee side of the island is, as was mentioned in the previous section, thermally induced, rather than by the effect of the topographic slope.

The complicated surface orography of the island makes it difficult to analyze the results quantatively, but some features of the results can be interpreted in terms of the linear wave model shown above. The island has two distinct ridges at the up- and downwind sides. While the island acts as a single isolated topographic barrier, the ridges on the island play their role as finite ridges. The wave motions shown in the vertical velocity and divergence fields (Figs. (3.4) and (3.5)) suggest that the wavelengths are determined by the length scales of the ridges.

Wurtele (1957) has shown that the disturbances generated by a three-dimensional topography resemble those by a two- dimensional topography following the lines of constant y, where y is the cross-stream coordinate. Hence his results, in their cross-sections at constant y planes, resemble those in a two-dimensional case presented by Lyra (1943). Figs. (3.9a,b) show

the solutions for a two-dimensional plateau (3.9a) by Lyra (1943) and for a three-dimensional plateau (3.9b) by Wurtele (1957).

It is clear in Figs. (3.4) and (3.5) that the amplitudes of the disturbances have their maximum values near the ground surface and decrease away from the island, vertically and horizontally.

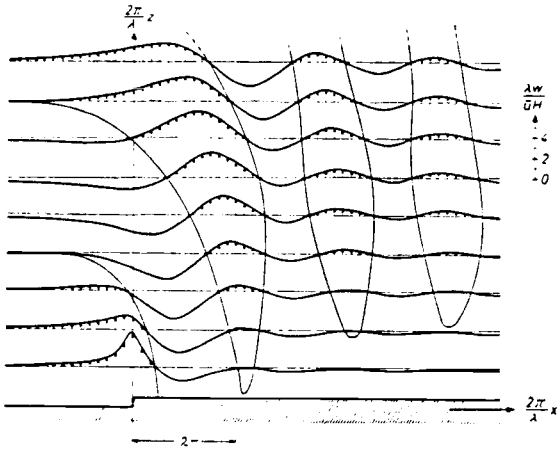

Fig. 3.9a Vertical velocities in the two-dimensional lee wave (after Lyra) where x is downstream distance, U the speed of mean flow, λ the horizontal wave length, and H is the height of the plateau.

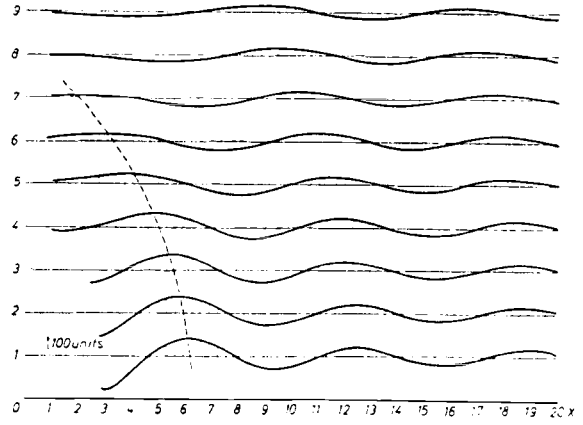

Fig. 3.9b Corresponding vertical velocities (in the y=0 plane) for the three-dimensional lee wave (after Wurtele).

The windward tilt of wave axis implies the vertical propagation of the wave energy. It has been shown by Smith (1980) that the amplitudes of the disturbances generated by a three-dimensional mountain decrease upwards proportional to $1/\sqrt{z}$ where z is the geometrical height above the topographic surface.

The wave motion at the lee side undergoes large variation in its magnitude and length scales with intense solar heating. This shows that thermal forcing is important during daytime at the lee side.

From Eqn. (3.8), the vertical wave length of a stationary wave is, with N=.01/sec, U=10m/sec, L=30km, and $\ell << k$, estimated to be approximately 6km. This estimate of the vertical wavelength is in good agreement with the model result.

In the vicinity of the island, the velocity perturbations have magnitudes comparable to the mean flow, and the linear theory can hardly be valid. The advective accelerations have non-negligible magnitudes in the vicinity of the island (Fig. (3.8)). And these advective accelerations appear to oppose the forcing by the pressure gradient in the lower atmosphere. But this effect of nonlinearity is beyond the scope of the present work.

Fig. (3.10) shows the diurnal variation of form drag and skin friction over the island surface. Form drag and skin friction appear to have comparable magnitude to each other and increase with increasing insolation during daytime. The increase of form

drag during daytime is a consequence of the intensification of low pressure at the lee side of the island, hence increase of pressure difference across the island. The sum of those two represents the total drag exerted on the atmosphere by the island and would be balanced by downward momentum flux. The momentum flux by the motions of a scale larger than one grid interval (not presented here) appears to be several orders of magnitude smaller than the total drag. Hence subgrid-scale momentum flux is expected to mainly balance the loss of momentum by form drag and skin friction while downward momentum flux by the waves is negligible.

The wave motions at the upwind side of the island may be either the artifacts of the cyclic lateral boundary or the traveling waves, or both. Linear theories do not predict any stationary wave activities in the upwind side of the mountain. Hence, if we consider that the instantaneous fields are presented as the model results, the traveling waves can appear in the figures. But no definite conclusions for these wave motions can be made in the present work, and the result needs further study with an open boundary model. It has been stressed by the previous authors (Queney, 1948; Wurtele, 1957; Smith, 1980, etc.) that correct radiation condition at the top of the domain is crucial to have correct wave solutions. Since the present study has imposed a solid upper boundary, the reflection of the wave energy at the top of the domain is expected to have affected the

results. While these effects cannot be determined quantitatively, future studies will have to carry correct radiation boundary conditions.

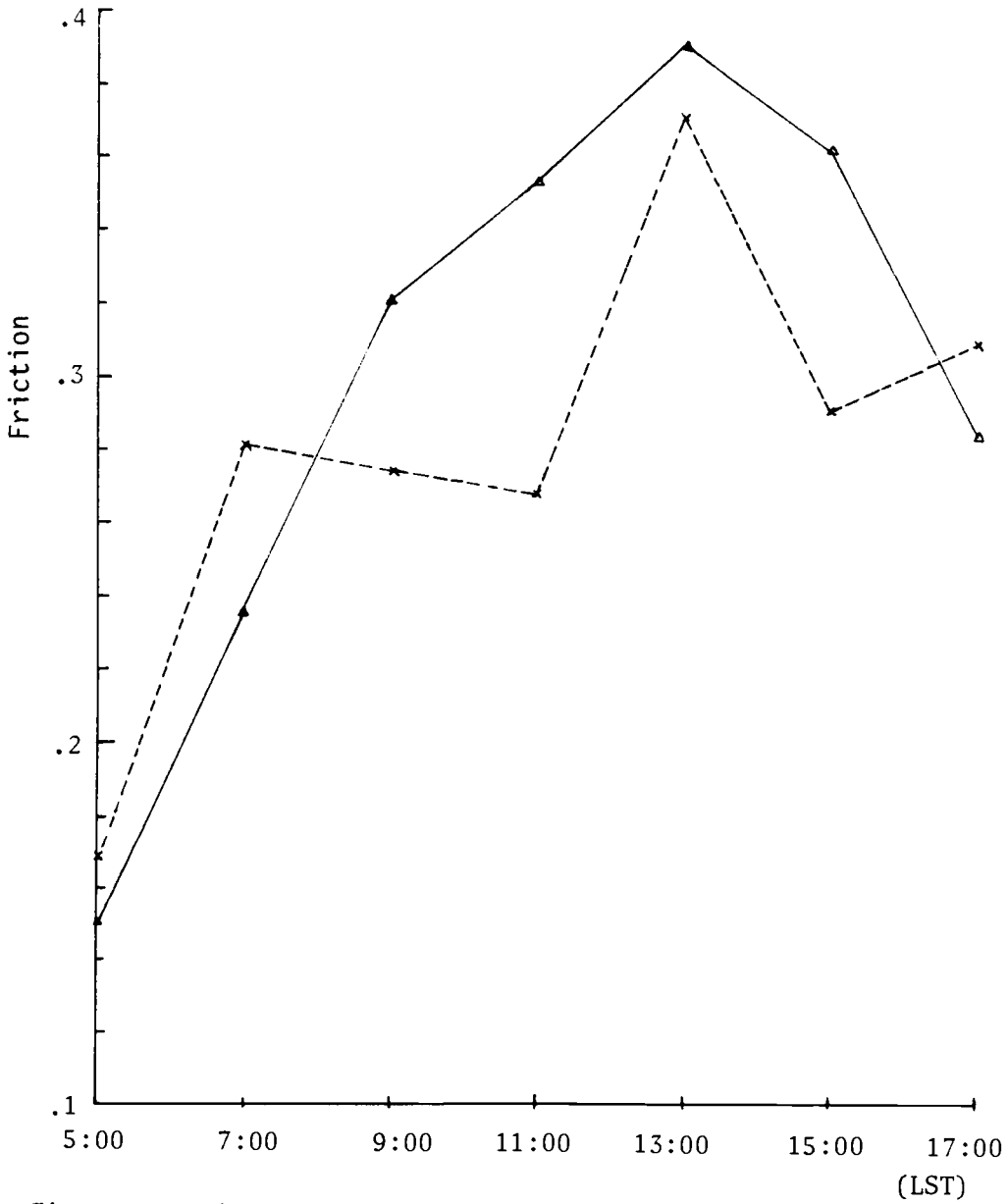

Fig. 3.10 Diurnal variations of form drag and skin friction. (dashed lines: form drag; solid lines: skin friction) The scale of the ordinate is N/m^2 (Pascal).

3-4 Comparisons of the Simulated Low-level Wind with the Observed Surface Wind

The climatology of the island of Oahu, Hawaii, has been well documented in earlier studies (Tracy et al, 1979). One of the best documented fields is the average rainfall data (Leopold et al, 1949). Although the rainfall can be related to the vertical motion, the lack of humidity variables in the present model makes it difficult to use the rainfall data to compare the model results. Rather, if we assume that the effects of condensation and precipation are small for a long term averaged wind, the observed near-surface wind field can be used for a comparison.

Fig. (3.11) shows the near-surface wind field from observations and present simulation. Solid arrows represent the mean observed wind at 12:00 LST, and dashed arrows represent the simulated wind at 13:00 LST. The mean observed wind field shown in Fig. (3.11) is an average surface wind for twelve trade-wind days of one year period, beginning from Aug. 1976 and ending at July 1977, presented in Tracy et. al. (1979). Daytime turning of the surface wind by the effect of solar heating of the island appears well both in the observed and simulated wind, especially at the points KP, WR, and BP in the figure.

While the overall feature of the low-level winds can be thought to be in good agreement, some systematic differences between the observed and simulated surface wind appear. It is

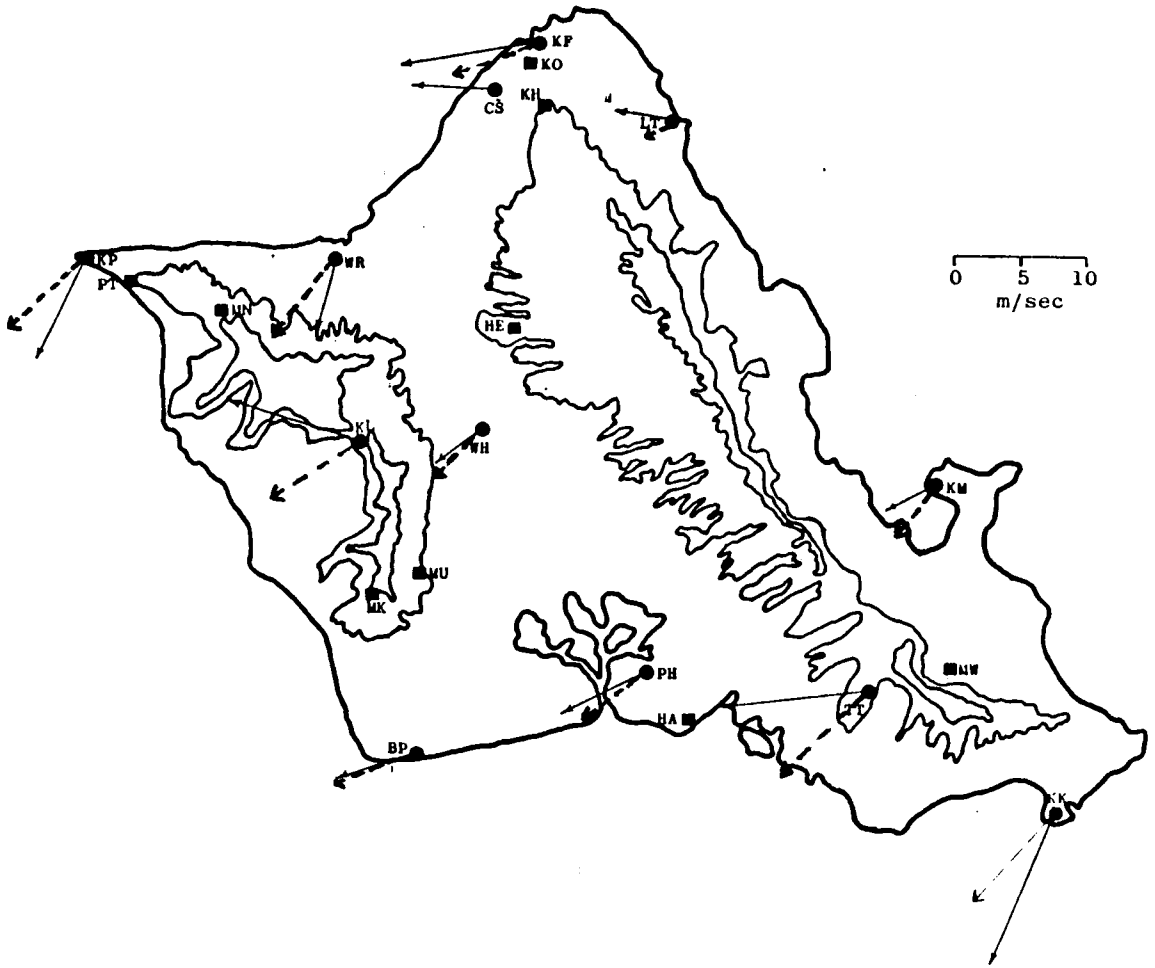

Fig. 3.11 Typical Tradewind data at 1200 LST based on average data (solid arrows) and the result of numerical simulation at 1300 LST (dashed arrows)

clear from Fig. (3.11) that the simulated wind field shows less variation in its direction and speed than the observed one over the island. Considering that the lowest-layer wind presented represents the average wind over a thickness of approximately 100m, this difference between the observed and simulated wind is acceptable. Another possibly important reason for this difference is that the model orography did not fully represent the real topography of the island. Especially, the large differences in the wind direction and speed at the points KL and TT are thought to be the consequence of errors in the representation of the real topography.

CHAPTER 4

Conclusions

The perturbations of a stably-stratified flow past an isolated island have been investigated utilizing a seven-layer, primitive-equation numerical model. The results suggest that topographic slopes and daytime heating of the island surface are the main factors which determine the flow field in the vicinity of the island. Asymmetric surface pressure, lateral deflection of incoming flow, and mass convergence at the lee side of the island all suggest that the results of the previous linear studies (e.g. Queney, 1948; Wurtele, 1957, and Smith, 1980) are valid, at least qualitativly. But some features, such as slowing down of incoming flow at the upwind side of the mountain, imply that nonlinearity is important in determining the local flow field.

During daytime, the flow field at the lee side and inland portion of the island is mainly determined by the pressure fluctuations caused by land-sea temperature contrast and cold-air advection from the ocean. Also, interaction of sea-breeze circulation with mean flow induces strong mass convergence and rising motion at the lee side of the island. But the effects of solar heating on the flow on the upwind side of the island appear to be small.

Main results of the present study are:

1) Asymmetric surface pressure, with high pressure at the upslopes and low pressure at the downslopes, arises due to vertical displacement of streamlines by topographic slopes when Fr>1.

2) The incoming flow diverges laterally and is slowed down by the high pressure at the upslope side of the island. Also, low pressure at the lee slope causes the streamlines to converge at the lee side.

3) Mixed layer thickness and potential temperature over the island increase downstream with maximum values at the lee side of the island.

4) During daytime, a well defined sea-breeze circulation arises at the lee side of the island and the interaction of sea breeze with mean flow causes strong rising motion at the lee side of the island.

5) Vertically propagating hydrostatic mountain waves are inferred to exist. But downward momontum flux associated with these waves appears to be negligible compared to total momentum loss by skin friction and hydrostatic form drag.

6) Skin friction and hydrostatic form drag have comparable magnitude to each other, and both increased with increasing insolation.

One of the serious deficiencies of the present model in studying mesoscale flow is the improper boundary conditions at the top of the domain as well as at the lateral boundaries. Reflection of wave energy at the top of the domain and re-input of the disturbances through cyclic lateral boundaries are expected to have affected the solution, but the effects cannot be determined quantatively at the present study. Hence future studies should employ open lateral boundaries and, possibly, non-reflecting upper boundary. Also, momentum and energy flux associated with mountain waves, hydrostatic form drag, and nonlinear effects should be explored in detail in future work.

REFERENCES

Arakawa, A. and V.R. Lamb, 1981: A potential enstrophy and energy conserving scheme for the shallow water equations. Mon. Wea. Rev., 109, 18-36.

Arakawa, A. and M.J. Suarez, 1983: Vertical differencing of the primitive equations in sigma coordinates. J. Mon. Wea. Rev., 111, 34-45.

Blackadar, A.K., 1979: High-resolution models of the planetary boundary layer. Adv. in environmental sci. and eng., vol 1, Gordon and Breach Science Publishers, 51-85.

Deardorff, J.W., 1971: On the magnitude of the subgrid scale eddy coefficient. J. Comput. Phys., 7, 120-133.

Deardorff, J.W., K. Ueyoshi, and Y.-J. Han, 1984: Numerical study of terrain-induced mesoscale motions and hydrostatic form drag in a heated, growing mixed layer. J. Atmos. Sci., 41, No.8, 1420-1441

Drazin, P.G., 1961: On the steady flow of a fluid of variable density past an obstacle. Tellus, 13, 239-251. Eliassen, A. and E. Palm, 1961: On the transfer of energy in stationary mountain waves. Geophys. Publ. Oslo, 22, No.3, 1-23.

Eliassen, A. and J.-E. Rekustad, 1971: A numerical study of meso-scale mountain waves. Geophys. Publ. Oslo, 28, No.3, 1-13.

Han, Y.-J., K. Ueyoshi, and J.W. Deardorff, 1982: Numerical study of terrain-induced mesoscale motions in a mixed layer. J. Atmos. Sci., 39, No.1, 2464-2476

Hyun, J.M. and M.-U. Kim, 1979: The effect of nonuniform wind shear on the intensification and reflection of mountain waves. J. Atmos. Sci., 36, 2379-2384.

Klemp, J.B. and D.K. Lilly, 1975: The dynamics of wave-induced downslope winds. J. Atmos. Sci., 32, 320-339.

Klemp, J.B. and D.K. Lilly, 1978: Numerical simulation of hydrostatic mountain wave. J. Atmos. Sci. 35, 78-106.

Lavoie, R.L., 1974: A numerical model of trade wind weather on Oahu. Mon. Wea. Rev., 102, 630-637.

Leopold, L.B., 1949: The interaction of trade wind and sea-breeze, Hawaii. J. Meteor., 6, 312-320.

Leopold, L.B., H. Landsberg, C.K. Stidd, T.C. Yeh, C.C. Wallen, J.E. Carson and J.J. Marciano, 1951: A group of papers: On the rainfall of Hawaii. 1, No.3, Meteor. Momogr. Amer. Meteor. Soc., Boston, 55pp.

Lilly, D.K., 1967: The representation of small-scale turbulence in numerical simulation experiments, in "Proceedings of the IBM Scientific Computing Symposium on Environmental Sciences", IBM Form No.320-1951. Louis, J.-F., 1979: A parametric model of vertical eddy fluxes in the atmosphere. Bound.-layer Meteor., 17, 187-202.

Louis, J.-F., M. Tiedke and J.F. Geleyn, 1982: A short history of the operational planetary boundary layer parameterization at ECMWF. Workshop on planetary bound. layer parameterization, European Centre for Medium Range Forecasts, 59-79, 260pp.

Lyra, G., 1943: Theorie der stationaren Leewellenstromung in freier Atmosphare. Z. angew. Math. Mech, 32, 1-28.

Mahrer, Y. and R.A. Pielke, 1975: A numerical study of the air flow over mountains using the two-dimensional versions of the University of Virginia mesoscale model. J. Atmos. Sci., 32, 2144-2155.

Mahrer, Y. and R.A. Pielke, 1977: A numerical study of the air flow over irregular terrain. Beit. Phys. Atmos., 50, 98-113

Messinger, F. and A. Arakawa, 1976: Numerical methods used in atmospheric models. GARP publication series, No.17, 1, WMO/ICSU Joint Organizing Committee, Geneva, 64pp.

Monin, A.S. and A.M. Obukhov, 1954: Basic laws of turbulent mixing in the atmosphere near the ground. Tr. Nank SSSR Geofiz. Inst., No.24(51), 163-187.

Phillips, N.A., 1974: Application of Arakawa's energy conserving layer model to operational weather prediction. NMC Note No.104, U.S. Dept. of Commerce, 40pp.

Pierrehumbert, R.T. and B. Wyman, 1985: Upstream effects of mesoscale mountains. J. Atmos. Sci., 42, No.10, 977-1003.

Queney, P., 1948: The problem of air flow over mountains: A summery of theoritical studies. Bull. Amer. Meteor. Soc., 29, 16-26.

Scorer, R.S., 1956: Airflow over an isolated hill. Quart. J. Roy. Meteor. Soc., 82, 75-81.

Smagorinsky, J.S., 1963: General circulation experiments with the primitive equations: I. The basic experiments, Mon. Wea. Rev., 91, 99-164.

Smith, R.B.,1980: Linear theory of stratified hydrostatic flow past an isolated mountain., Tellus, 32, 348-364.

Suarez, M.J. and A. Arakawa, 1979: Description and priliminary results of the 9-level UCLA general circulation model, Fourth conf. on Num. Wea. Prediction. Silver Spring, Amer. Meteor. Soc., 290-297.

Tracy, R.M. and G.T. Phillips and K.C. Rock, 1979: Wind energy siting methodology wind field model verification program: I. Oahu, Hawaii, Data set. Interim. Report for the period September 15, 1978-April 15, 1979., U.S. Dept. of energy, 133 pp.

Ueyoshi, K., 1985: Numerical simulation of planetary boundary-layer evolution and mesoscale flow over irregular terrain under daytime heating conditions., Ph.D thesis, Dept. AtS., Oregon State University, 282pp.

Wurtele, M.Gg., 1957: The three-dimensional lee wave. Beit. zur Phy. der Atmos, 29, 5, 242-252.